Urban Water Research Association of Australia

Numerical Modelling of Extreme Precipitation Events

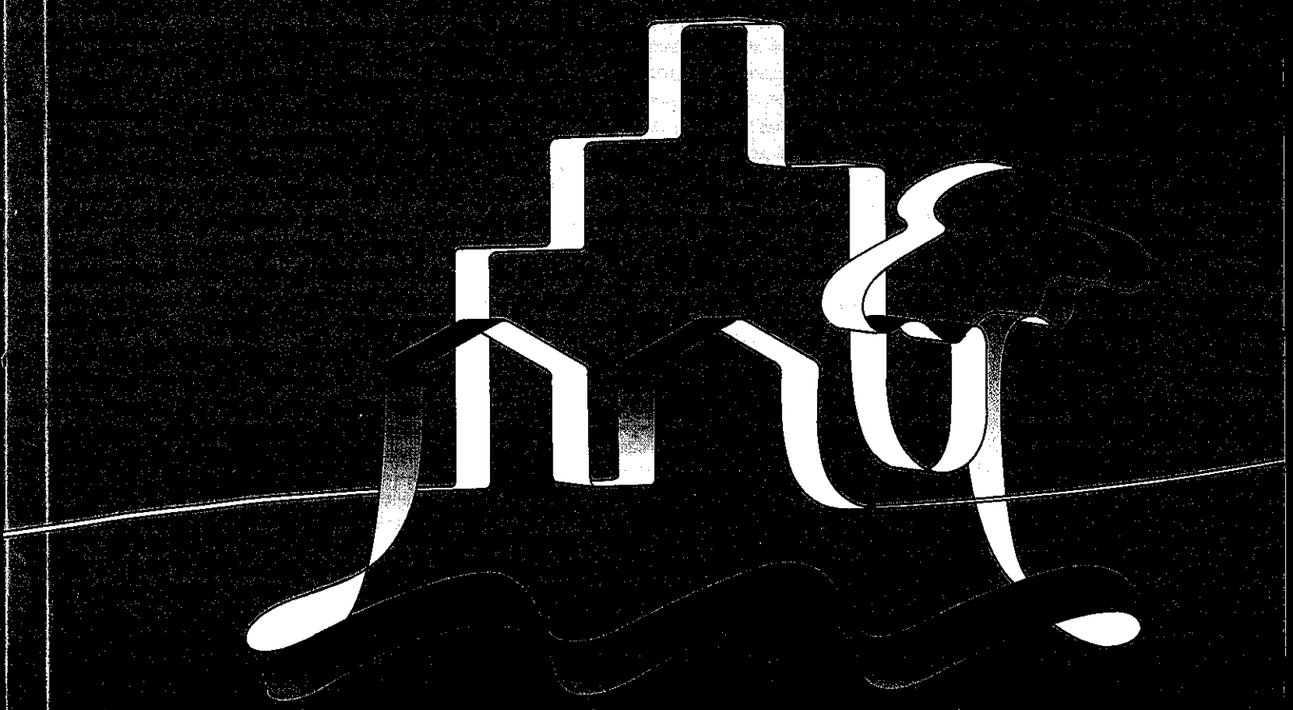

URBAN WATER RESEARCH ASSOCIATION OF AUSTRALIA (UWRAA)

The Association is a Division of the Water Services Association of Australia. UWRAA has the charter to develop and manage a portfolio of research to support the business plan for the urban water industry developed by the Water Services Association of Australia.

The UWRAA Research Report series presents information resulting from research projects supported by the Association and is published as a record of the work undertaken and as a means of disseminating the research findings. The Association also encourages the presentation of findings by the researchers in professional journals and at conferences. The Association's reports are indexed on STREAMLINE, the national water data base.

For further details contact:
Dr John Langford
Executive Director
Water Services Association of Australia
Level 7
469 Latrobe Street Telephone: (03) 9606 0678
Melbourne Vic 3000 Fax: (03) 9606 0376

Urban Water Research Association of Australia

Numerical Modelling of Extreme Precipitation Events

D J Abbs and B F Ryan

CSIRO Division of Atmospheric Research

Research Report No 131
December 1997

ISBN 1 876088 37 0

Foreword

This report is based on UWRAA Research Project No WR-22: 'Numerical Modelling of Extreme Precipitation Events' which was undertaken during the period July 1992 - July 1997. Organisational responsibility for the project was as follows:

Sponsoring Authority:	Sydney Water Board
Project Officer:	Dr Brian Ryan CSIRO Division of Atmospheric Research PMB No 1 Aspendale, Vic 3195
Research Agency:	CSIRO
Principal Researcher:	Dr Debbie Abbs CSIRO Division of Atmospheric Research Aspendale, Vic

The project was funded by CSIRO Division of Atmospheric Research and the Urban Water Research Association of Australia.

Executive Summary

Background

The Urban Water Research Association of Australia research grant WR-22 has been used to investigate whether numerical models of the atmosphere may be used as tools for quantitative precipitation forecasting, over catchment size regions, for extreme precipitation events. This report documents the investigation and its outcomes.

The concept of PMP, or Probable Maximum Precipitation, is used by hydrologists and meteorologists involved in the design of structures, such as dams or bridges, where the need is to compute extreme rainfall (and hence flood) events. The concept is that the PMP is an upper bound for rainfall at a site. It is thus seen as a single deterministic number (governed by physical principles) that would never be exceeded. However, there have been several occasions on which observed rainfalls have exceeded PMP estimates valid at the time; the occurrence of such events led to a re-evaluation of the PMP methodologies and resulted in the development of the generalised techniques that are now used throughout Australia.

A more practical problem associated with an increase in past PMP estimates is that, if the original PMP estimates are subsequently revised upwards, this will involve expensive remedial works to upgrade under-designed spillways. In recent times hydrologists have called for a reappraisal of the philosophies underlying dam safety practices (e.g. Laurenson and Pearse, 1991).

Consequently, there has been pressure to validate independently and to improve the current PMP methodology. The major rationale for this project was to provide the first steps towards using numerical modelling techniques to enhance the current PMP procedures.

Aims of this Research Project

The aim of this research project has been to develop a technique, using numerical mesoscale atmospheric models, to evaluate independently the assumptions used in the simple two parameter conceptual model that is used for Probable Maximum Precipitation calculations. These assumptions are:

(1) the precipitation is linearly related to the precipitable water;

(2) the precipitation efficiency of the storm does not change as the moisture available to the storm increases;

(3) terrain "modulates" the distribution of the precipitation but does not affect the synoptic-scale dynamics of the storm.

The following steps are used to evaluate the assumptions detailed above:

(1) use a numerical model of the atmosphere to simulate recent large storms;

(2) compare the model results with the observed rainfall and storm development;

(3) carry out sensitivity analyses to determine the maximum precipitation efficiency of the storms;

(4) develop a hypothetical "worst case storm" that would allow a comparison between the model generated Depth-Duration-Area (DDA) curves and the DDA curves calculated using the maximisation relationship of the current generalised technique.

- **Numerical Models of the Atmosphere**

Numerical models of the atmosphere solve the three-dimensional equations of motion, the thermodynamic equation and the moisture equation. This is achieved by converting these equations to finite difference form and solving them on a regular three-dimensional grid that covers the geographic region of interest. As the grid spacing used in the solution of these equations is decreased, the corresponding time step must be decreased to maintain computational stability.

Extreme precipitation events are usually convective in nature requiring the updraft/downdraft cores to be resolved. Observations show that in major convective systems, ranging from thunderstorms to tropical cyclones, the updraft/downdraft cores are on the scale of 3-5 km or less (e.g. Zipser and Lemone, 1980). The characteristics of these cores require that the model be non-hydrostatic. On the other hand, these cores are embedded in larger synoptic systems. The computing requirements to model the full extent of the synoptic system at a horizontal resolution of 1-2 km is prohibitive. The model must therefore be nested, that is, the large scale flow must be modelled at lower resolution and used to force the boundaries of the high resolution simulation (see Figure 1, page 8). The model orography must be realistic and consistent with the resolution used in the simulation.

It is essential that the model represents realistically sub-grid scale processes. These include the parameterisation of the important surface processes, such as evaporation and heating. The parameterisation of radiation must therefore include the diurnal heating and cooling cycle, as well as the interaction of the long and short wave radiation with the clouds. Mixing in the boundary layer must be parameterised to take account of turbulence and shallow convection. The parameterisation of deep convection requires the use of a convective parameterisation scheme that is suitable for use at horizontal grid resolutions of 5-10 km. Finally the model needs to represent the cloud and rain generating processes in the atmosphere.

In addition, the initial conditions need to be thermodynamically and physically consistent to prevent instabilities and errors developing as the simulation proceeds. For example, if the thermodynamic fields and mass fields are inconsistent, then the model may experience an initial "shock" that may develop and dominate the solution. Good meteorological observations and analyses are therefore essential for the simulation exercise, being needed both to initialise the model and to validate the simulation prior to the maximised simulations. In Australia the most dense meteorological networks are on the eastern seaboard; for this reason, this is a preferred region to test the technique.

The Colorado State University Regional Atmospheric Modeling System (RAMS) meets the requirements discussed above and was the tool chosen to test the applicability of the modelling technique to PMP applications. These techniques have been tested on four case studies: (i) an east-coast low, (ii) an upper-level cut-off low, (iii) a west Australian tropical cyclone, and (iv) an east Australian tropical cyclone. For each of these case studies we have investigated the effect increases in the moisture availability have on the precipitation produced by the storm, on

the precipitation efficiency of the storm and on the depth-duration-area analyses for the storm. We have also investigated the effect of terrain on the precipitation produced by the east-coast low and upper-level cut-off low.

Study Results

In this report we have shown that numerical models can be used for quantitative precipitation forecasting (QPF) of southeastern Australian storms (storms (i) and (ii)) and may provide useful results at a horizontal resolution 5-10 km. A number of similarities exist between the two case studies presented here. Both case studies show that the systems are 70-80% efficient at generating moderate rainfall (rainfall rates less than 25 mm hr^{-1}) and that heavy rainfall production is 80-90% efficient. In the case of southeastern Australian storms long-lived, rain processes under conditions of moderate rainfall are important contributors to the total precipitation produced by the storm. Increases in the moisture availability result in the rainfall beginning earlier, lasting longer and being more continuous.

Terrain effects are shown to influence both the amount of rainfall that occurs over the higher terrain and the distribution of rainfall due to the "convergence component" of the storm. This is due to changes in the movement of the storm or changes in the low-level wind field (e.g. blocking) when terrain effects are neglected. The temporal variation of the precipitation for these simulations also illustrates that changes in the moisture field feeds back to the dynamics by affecting both the intensity and movement of the storm.

We have also shown that the numerical model is able to reproduce many of the high resolution features of tropical cyclones provided that high quality analyses are available with which to initialise the model. We have found that sophisticated initialisation ("vortex bogussing") techniques should be employed to simulate such features as the formation of a radius of maximum winds, the "spin-up" of the tropical cyclone and a better prediction of the track. Despite these shortcomings, the model is able to provide an adequate prediction of the precipitation field, even at a horizontal resolution of 15 km, against which to test some of the PMP estimation assumptions.

For tropical cyclones Connie and Aivu, both moderate and heavy rainfall are generated efficiently. For all simulations, the generation of heavy rainfall is almost 100% efficient. The precipitation efficiency shows little sensitivity to increases in the moisture available to the storm. As the moisture available to the storm is increased, the heavy rainfall becomes more continuous and longer lived.

Study Conclusions

Five conclusions with implications for the estimation of PMP may be drawn from the work presented in this report.

1. As the moisture availability is increased the precipitation efficiency of the storms does not change significantly. For each case study presented, the production of heavy rainfall (rainfall rates greater than 25 mm hr^{-1}) is between 80% and 100% efficient. This supports the simple model that assumes implicitly that extreme precipitation storms have the highest efficiency.

2. As moisture availability is increased the duration of the heavy rainfall increases, i.e. it begins earlier and is more continuous. Life cycles are not considered in the simple model; however, the results presented here and the recent paper of Zhao *et al.* (1997) suggest that the duration of the storm increases as the moisture availability increases. An increase in the duration of heavy rainfall will result in higher total rainfall.

3. As moisture availability changes, the spatial distribution of the area over which more than 50% of the total rainfall occurs as heavy rainfall changes. Zhao *et al.* (1997) also found that the areal coverage of rainfall varies nonlinearly with the precipitable water.

4. The control simulation may be thought of as giving the depth-area curve for the actual storm, while the enhanced-moisture simulation provides the depth-area curves for a storm maximised by the moisture while conserving its dynamic integrity. The enhanced moisture storm is associated with a moisture-adjustment factor and the current PMP methodology would multiply the depth-area curves of the control simulation by this factor. If the depth-area curve for the increased moisture simulation lies above that of the control simulation, then the maximisation relationship of the current PMP technique under-estimates the precipitation simulated by the model. The simulations reported here indicate that this may occur and hence the precipitation is not linearly related to the precipitable water. Where this was the case, for the case studies presented in Section 3, the model produces between 15% and 35% more precipitation than the current storm maximisation technique for areas of 50 to 70 km^2. For areas of 500 km^2, the model produces between 5% and 15% more precipitation then the current storm maximisation technique.

5. The topography affects the distribution of the "convergence component" of the precipitation due to feedback effects to the dynamics of the storm system.

Despite these deficiencies in the assumptions used to estimate PMP, we believe that there is no operational replacement available at present for the current PMP methodology. However, improvements in the estimation of PMP may soon be possible if increased effort is placed on (amongst other things) the numerical modelling of extreme rainfall events. These improvements are only possible if the results of these efforts are communicated to, and accepted by, the hydrological community.

Suggested Extensions to this Work

As computing capabilities increase, it will become possible to model extreme storms at increasingly higher resolution. The advances in computing hardware make it possible to examine whether increasing the horizontal resolution of the simulated storms affects the above conclusions. In addition, more case studies should be attempted to determine if the above conclusions hold true for these cases.

The natural extension of this project is to use the model-predicted precipitation fields to provide an "observed" precipitation field and then subject them to the analysis given to the extreme storms that constitute the GSAM database. After the application of identical maximisation factors, the results of the maximised storm should be compared with that of the equivalent simulated "increased moisture" storm.

When this project began 5 years ago it was possible only to perform these simulations on very expensive supercomputers. The continual increase in computing capabilities means that these simulations may now be performed on moderately sized (and priced) workstations. In addition, a number of re-analysis projects are in progress (e.g. National Centers for Environmental Prediction (NCEP) in the USA and at the European Centre for Medium-Range Weather Forecasts (ECMWF)) to upgrade the old analyses using state-of-the-art general circulation models and including observations that were not available when the models were originally run. These re-analysis projects are thus providing an improved dataset with which to initialise mesoscale numerical models. In the NCEP case the re-analysis extends back to 1970s and so a larger storm database will be available soon.

Finally, the physical parameterisation schemes incorporated into mesoscale numerical models are continually improving, resulting in high quality simulations of these events at increasingly higher horizontal resolution. However, these models are very complex and require a skilled meteorological modeller to manage them and to interpret the results - they cannot be used as a "black box".

Consequently, we believe that it is becoming possible to perform simulations of a greater number of extreme rainfall events and to provide skilful quantitative precipitation forecasts of them. By utilising a "team approach", in which hydrometeorologists and meteorological modellers work together, it is now possible to use mesoscale numerical models as tools for hydrological planning.

Table of Contents

1. Introduction

The Urban Water Research Association of Australia research grant WR-22 has been used to investigate whether numerical models of the atmosphere may be used as tools for quantitative precipitation forecasting, over catchment size regions, for extreme precipitation events. This report documents the investigation and its outcomes.

1.1 Statement Of Problem

The concept of PMP, or Probable Maximum Precipitation, is used by hydrologists and meteorologists involved in the design of structures, such as dams or bridges, where the need is to compute extreme rainfall (and hence flood) events. The concept is that the PMP is an upper bound for rainfall at a site. It is thus seen as a single deterministic number (governed by physical principles) that would never be exceeded. However, there have been several occasions on which observed rainfalls have exceeded the PMP estimates valid at the time; the occurrence of such events led to a re-evaluation of the PMP methodologies and resulted in the development of the generalised techniques that are now used throughout Australia.

A more practical problem associated with an increase in PMP estimates is that, if the original PMP estimates are subsequently revised upwards, this will involve expensive remedial works to upgrade under-designed spillways. In recent times hydrologists have called for a reappraisal of the philosophies underlying dam safety practices (e.g. Laurenson and Pearse, 1991). In the United States, a recent study (National Research Council, 1994) noted the importance of developing improved hydrometeorological analysis procedures for assessing extreme precipitation. Stewart (private communication, 1997) notes the need to "develop a consistent methodology for estimating PMP that accounts for the natural variability of climate and our relatively short historical records."

Consequently, there has been pressure to validate independently and to improve the current PMP methodology. The major rationale for this project was to provide the first steps towards using numerical modelling techniques to enhance the current PMP procedures.

1.2 Background

Because of the potential hazards associated with over-topping of large dams, a high degree of security in the calculation of the spillway design flood is required. The Australian National Committee On Large Dams (ANCOLD, 1986) defines the Annual Exceedance Probability (AEP) to be the probability that a particular flood value will be exceeded in any year.

In Australia, the AEP of the design flood is estimated from the frequency analysis of flood records, all of which are typically less than 100 years in duration. This method of analysis can provide reliable AEP estimates only down to about 10^{-2} and certainly insufficient security for a

large dam. The design of large dams is based on the much more conservative estimate of the Probable Maximum Flood (PMF), which in turn depends on the estimate of the PMP.

PMF is estimated using a design storm method based on the PMP. In turn, PMP has been historically estimated in a variety of ways using techniques that maximise recorded storms. When the storms maximised are only those that occur on the catchment under consideration the method is called the "in-situ maximisation" method. When storms that occur in adjoining and geographically similar regions to the catchment area are also considered the method is called the "transposition and maximisation method".

Hart (1982) shows the physical basis for storm maximisation is based on a simple two parameter model of the storm, derived as follows. A storm is considered to consist of a convergent mass flow at low levels that rises and diverges in an upper outflow layer. The water vapour budget equation associated with the storm can be written as

$$E - P = \int \left[\frac{\partial q}{\partial t} + \nabla.(qV) \right] \frac{dp}{g} \qquad (1)$$

where E is evaporation, P is precipitation, q is specific humidity, V is the horizontal wind vector, g is the acceleration due to gravity and the vertical integration is carried out over the depth of the atmosphere. For major storms it is assumed that the evaporation term E, the rate of water vapour storage term $(\partial q/\partial t)$, and the moisture gradient in the vicinity of the storm are negligible. With these assumptions Equation (1) can be rewritten as

$$P = -\int q \nabla.V \frac{dp}{g}, \qquad (2)$$

that is, the rainfall rate is approximately equal to the vertically integrated product of the mass convergence and the specific humidity. If the model is further simplified to comprise an inflow layer Δp_1 and an outflow layer Δp_2 with uniform divergences D_1 and D_2 and specific humidities q_1 and q_2, the precipitation, P, reduces to

$$P = -\left(\frac{q_1 \Delta p_1 D_1 - q_2 \Delta p_2 D_2}{g} \right). \qquad (3)$$

From considerations of mass continuity, $\Delta p_1 D_1 = \Delta p_2 D_2$ and $q_1 >> q_2$, and hence the precipitation is approximated by

$$P \approx -\frac{q_1 \Delta p_1 D_1}{g}. \qquad (4)$$

To calculate the maximised precipitation the product of the moisture inflow and mass convergence needs to be maximised. The term $q_1 \Delta p_1$ is the effective precipitable water, w_e, for a storm and this can be maximised by using 24-hour persisting dew points to calculate a maximum effective precipitable water, $w_{e_{max}}$. The maximised precipitation is then calculated by

adjusting the observed rainfall by a moisture adjustment factor $w_{e_{max}}/w_e$. However, as pointed out by Weisner (1970), it is common practice to calculate the moisture adjustment factor from the actual precipitable water in a saturated atmospheric column, and the maximised precipitable water (w_{max}) as given by the maximum 24-hour persisting dew points. The dew point uniquely defines the mixing ratio at cloud base and therefore the precipitable water in the saturated column. This indirect technique arises because there is usually no way of characterising the extreme mass convergence, so the observed rainfall is taken as an implicit measure of this quantity. It is assumed that extreme precipitation storms have the highest efficiency. The maximised precipitation is thus calculated from the precipitable water w, derived from the observed dew point, the maximised precipitable water w_{max}, and the observed rainfall P (normally in the form of Depth, Duration and Area [DDA] curves) as

$$P_{max} = \left(\frac{w_{max}}{w} \right) \times P. \qquad (5)$$

More recently, a technique known as the "generalised method" has been developed to calculate the PMP. Generalised methods use rainfalls recorded over a large region and from a large database of storms. The storm database is generalised by separating out that portion of the rainfall attributable to regional meteorological conditions from that which may be considered to be due to site-specific (e.g. topography) characteristics. These techniques help overcome the problems associated with the shortness of Australia's rainfall record and provide regionally consistent (Pearce and Kennedy, 1994) estimates of the PMP. The Australian Bureau of Meteorology has developed three generalised methods that are applicable to the country. The first is the Generalised Short Duration Method (GSDM), the second is the Generalised Tropical Storm Method (GTSM) and the third is the Generalised Southeastern Australia Method (GSAM). The GSDM is applicable for small areas up to 1000 km^2 and for time periods up to 6 hours. The GTSM and the GSAM are used for larger areas of the order of 10^4 km.

A brief description of the GSAM is given below, since it provides an introduction to the research described in this report. The GSAM was developed for use in large catchments in southeast Australia. The GSAM is based around a catalogue of 110 storms covering the period from 1889 to 1990. Following the creation of the GSAM storm catalogue, each storm was gridded and temporal distributions of the total storm rainfall determined. These temporal distributions are defined as "the maximum percentages of the total storm rainfall that fell within the standard durations and the standard areas". The depth-area curve for the total storm duration was calculated and the depths at the standard areas were determined by interpolation. These were then multiplied by the percentage depths from the temporal distributions to produce a set of depth-area curves at standard durations and areas. The technique of moisture maximisation requires knowledge of the moisture content of the storm. The precipitable water is used as a measure of this quantity and is determined from the 1000 hPa dewpoint temperature representative of the storm. The estimation of the dewpoint temperature is very subjective and Minty *et al.* (1996) estimate that an accuracy of about 2°C only is possible.

The storm database is generalised by identifying and removing the site-specific features of each storm so that the storm may be transposed to other locations. These features are storm type, spatial distribution, topographic influences and moisture content. By dividing the country into

various regions and zones, the effects of storm type were removed from the database. The spatial distribution of each storm was removed by quantifying each storm in terms of a set of depth-duration-area curves. A unique feature of the GSAM is the technique developed to estimate the topographic component of the rainfall. It is assumed that precipitation results from the convergence and vertical motion of moisture air and that these motions are due to either synoptic-scale disturbances or topographic influences. Precipitation due to synoptic-scale disturbances, such as frontal lifting, and any atmospheric process unaffected by terrain, is termed the "convergence component" of the storm. The remainder of the precipitation is attributed to topographic influences and termed the "topographic component". The recorded storm rainfall was separated into convergence and topographic components and the convergence component maximised using (5), where w_{max} is the extreme precipitable water associated with the extreme 24 hr persisting dewpoint temperature recorded for the storm location and time of year. Moisture maximisation thus removes the storm-specific feature of moisture content. The site-specific feature of moisture content is removed by standardising the moisture content to the standard extreme dewpoint temperature for the zone and season, in a manner analogous to storm maximisation. Standardisation is only valid for the convergence component of the storm. The final step in generalising the database is to draw an enveloping curve to the maximised, standardised convergence component depth-area curves for each season and duration. For each season, these curves are representative of a single hypothetical storm of maximum moisture content and maximum efficiency.

To apply the method to a particular catchment, the convergence component for each season is obtained from the envelope value for the appropriate season and catchment size, then multiplied by the moist adjustment factor corresponding to the season. The catchment PMP convergence component is defined as the maximum of these depths across all seasons. To account for the topographic influence of the chosen catchment, the catchment PMP convergence component is then multiplied by the catchment PMP topographic enhancement factor to produce the PMP value for each duration. The reader is referred to Minty *et al.* (1996) for a complete discussion of the development of the generalised method for southeast Australia.

1.3 Objectives

The aim of this research project has been to develop a technique, using numerical mesoscale atmospheric models, to evaluate independently the assumptions used in the simple two parameter conceptual model that is used for PMP calculations.
These assumptions are :

(1) the precipitation is linearly-related to the precipitable water (i.e. $P_2 = \left(\frac{w_2}{w}\right) \times P$);

(2) the precipitation efficiency of the storm does not change as the moisture available to the storm increases;

(3) terrain modulates the distribution of the precipitation but does not affect the synoptic-scale dynamics of the storm.

The relationship between the precipitable water and the precipitation (assumption 1) is particularly important since it is this relationship that underlies the foundations for both moisture maximisation and storm transposition. The report of the National Research Council (1994) also concludes that the scientific foundations of the traditional PMP procedures, such as moisture maximisation and storm transposition, require detailed study. That report points to numerical models as key tools for enhancing PMP procedures.

The following steps are used to used to evaluate the assumptions detailed above.

(1) use a numerical model of the atmosphere to simulate recent large storms;

(2) compare the model results with the observed rainfall and storm development;

(3) carry out sensitivity analyses to determine the maximum precipitation efficiency of the storms;

(4) develop a hypothetical "worst case storm" that would allow a comparison between the model generated Depth-Duration-Area (DDA) curves and the DDA curves calculated using the maximisation relationship of the current generalised technique.

1.4 Guide to this report

Section 2 describes the methodology used to evaluate the above assumptions. The requirements of a numerical model that simulates extreme precipitation events are also discussed in that section. Four case studies have been completed. Case studies of two southeastern Australian storms are presented in Section 3 and case studies of two tropical cyclones are presented in Section 4. For each case study, the simulated storm is validated and other simulations are presented to determine the sensitivity of the storm to changes in the moisture availability. Precipitation efficiencies and depth-duration-area analyses are calculated for each storm and its increased moisture counterpart. The outcomes and future applications of this work are discussed in Section 5. A glossary of acronyms is provided in Section 9.

2. Methodology

In this Section it will be assumed, (i) that it is possible to model accurately extreme storms using a mesoscale numerical model of the atmosphere, and (ii) the model can simulate realistically the amount and distribution of precipitation on the catchment scale. We will address the validity of these assumptions in Sections 3 and 4.

Step 1: Model Validation

The first step is to show that the numerical model being used is capable of simulating observed extreme storms and then to compare the simulated Depth-Duration-Area (DDA) curves with observations. The model simulations need to be classified according to synoptic systems. In developing this methodology, the current Bureau of Meteorology generalised storm categories of (a) short duration thunderstorms, (b) southeastern Australian storms and (c) tropical storms are the appropriate classifications. Short duration thunderstorms that lead to flash flooding need to be validated against observed extreme thunderstorms. By contrast, in those areas of northern Australia where the flooding is generated by synoptic depressions or tropical cyclones, a different family of simulations will be required and the modelling constraints might well be different.

Step 2: Comparison with the simple two parameter moisture maximisation model

The fundamental assumption in the two parameter physical model is that both parameters (the moisture inflow and the low-level convergence) are independent. A major aim of this project is to use the numerical simulation to test the validity of this assumption. It is assumed that in an extreme storm the low-level convergence is maximised but that the moisture is not, so the maximised storm can be derived by maximising the moisture inflow. The modelling studies are able to test directly this hypothesis by repeating the simulation after maximising the moisture inflow to the storm. In addition, the increased model rainfall can be compared with the maximised precipitation calculated from the generalised technique (see Equation 5). In this study, the moisture values have been increased by uniformly increasing the temperatures of the atmosphere everywhere, while maintaining the relative humidities. In this way the system is still in dynamic balance but the specific humidity, and hence precipitable water, has been increased. The maximisation factor is defined as the ratio of the precipitable water for the increased moisture simulation to the precipitable water for the control simulation. The maximisation factor is determined for those portions of the storm for which the atmosphere is saturated. This method is comparable to the technique used to maximise storms in the current generalised approach.

Step 3: Sensitivity to increases in the moisture availability and topography.

An advantage of using numerical models is that the model is able to simulate complex, non-linear processes that cannot be represented realistically otherwise. Such process include, for example, changes in the convective processes as the moisture available to the storm increases, and the effect of terrain on the wind field and hence on the location and timing of the rainfall. By performing an ensemble of simulations in which the moisture availability to the storm is changed, it is possible to determine some of these effects. Similarly, it is possible to perform

simulations in which the effects of terrain are removed to investigate the development of the modelled storm under these hypothetical conditions.

2.1 Requirements of a model for PMP studies

In the previous Section it was implicitly assumed that extreme precipitation events can be modelled with the current generation of numerical mesoscale atmospheric models. Numerical models of the atmosphere solve the three-dimensional equations of motion, the thermodynamic equation and the moisture equation. This is achieved by converting these equations to finite difference form and solving them on a regular three-dimensional grid that covers the geographic region of interest. As the grid spacing used in the solution of these equations is decreased, the corresponding time step must be decreased to maintain computational stability. In this section we will examine the requirements for a numerical model that simulates extreme precipitation events.

(a) Resolution and Orography

Extreme precipitation events are usually convective in nature requiring the updraft/downdraft cores to be resolved. Observations show that in major convective systems, ranging from thunderstorms to tropical cyclones, the updraft/downdraft cores are on the scale of 3-5 km or less (e.g. Zipser and Lemone, 1980). The characteristics of these cores requires that the model be non-hydrostatic. On the other hand, these core are embedded in larger synoptic systems. The computing requirements to model the full extent of the synoptic system at a horizontal resolution of 1-2 km is prohibitive. The model must therefore be nested, that is, the large scale flow must be modelled at lower resolution and used to force the boundaries of the high resolution simulation (see Figure 1). The model orography must be realistic and consistent with the resolution used in the simulation.

(b) Physical Processes

It is essential that the model represents realistically sub-grid scale processes. These include the parameterisation of the important surface processes, such as evaporation and heating. The parameterisation of radiation must therefore include the diurnal heating and cooling cycle, as well as the interaction of the long and short wave radiation with the clouds. Mixing in the boundary layer must be parameterised to take account of turbulence and shallow convection. The parameterisation of deep convection requires the use of a convective parameterisation scheme that is suitable for use with horizontal grid resolutions of 5-10 km. Finally, the model needs to represent the cloud and rain generating processes in the atmosphere.

(c) Realistic Analyses

In addition, the initial conditions need to be thermodynamically and physically consistent to prevent instabilities and errors developing as the simulation proceeds. For example, if the thermodynamic fields and mass fields are inconsistent, then the model may experience an initial "shock" that may develop to dominate the solution. Good meteorological observations and analyses are therefore essential for the simulation exercise, being needed both to initialise the storm and to validate the simulation prior to the maximised simulations. In Australia the most

dense meteorological networks are on the eastern seaboard; for this reason, this is a preferred region to test the technique.

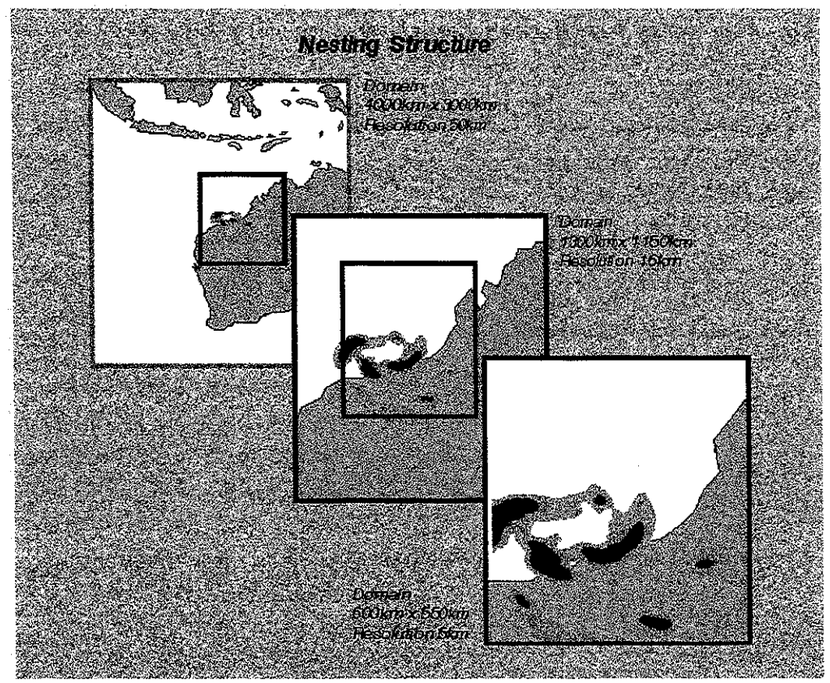

Figure 1: The 2-way nested regions used in the RAMS simulation of Tropical Cyclone Connie.

2.2 Colorado State University Regional Atmospheric Modeling System

The Colorado State University Regional Atmospheric Modeling System (RAMS) meets most of the requirements discussed above and was the tool chosen to test the applicability of the modelling technique to PMP applications. Details of the RAMS model can be found in Tremback *et al.* (1986). It was necessary to couple RAMS to a convective parameterisation scheme that was suitable for use at resolutions of the order of 10 km. The convective parameterisation scheme chosen was that of Frank and Cohen (1985, 1987).

The model has been used to simulate the passage of a cold front over the Thomson Dam catchment area in Victoria where it gave a good distribution of the rainfall (Ryan and Abbs, 1991). Figure 2 shows the observed and model results for the Thomson Dam simulation. Further observational and modelling studies by Abbs and Jensen (1992) have shown that the model realistically calculates both the in-cloud structure of the clouds that form over Mount Baw Baw and the rainfall into the Thomson River catchment area. These results show that for this simulation, RAMS correctly models the atmospheric portion of the water cycle for this storm. The simulations described herein require large computing resources, both in terms of central processing power and data storage. Examples of these requirements are given in the appendix.

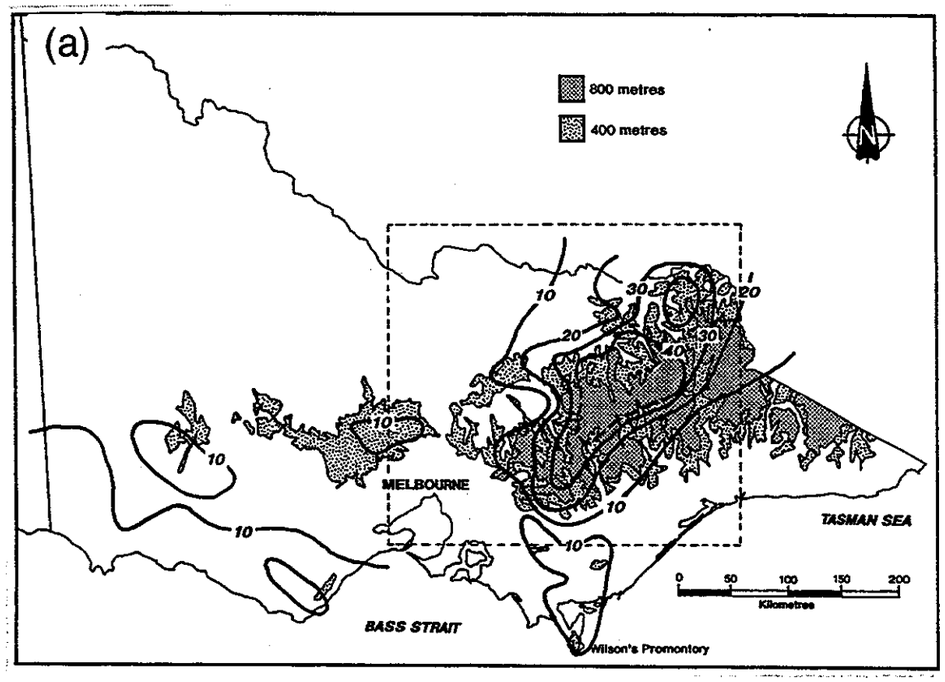

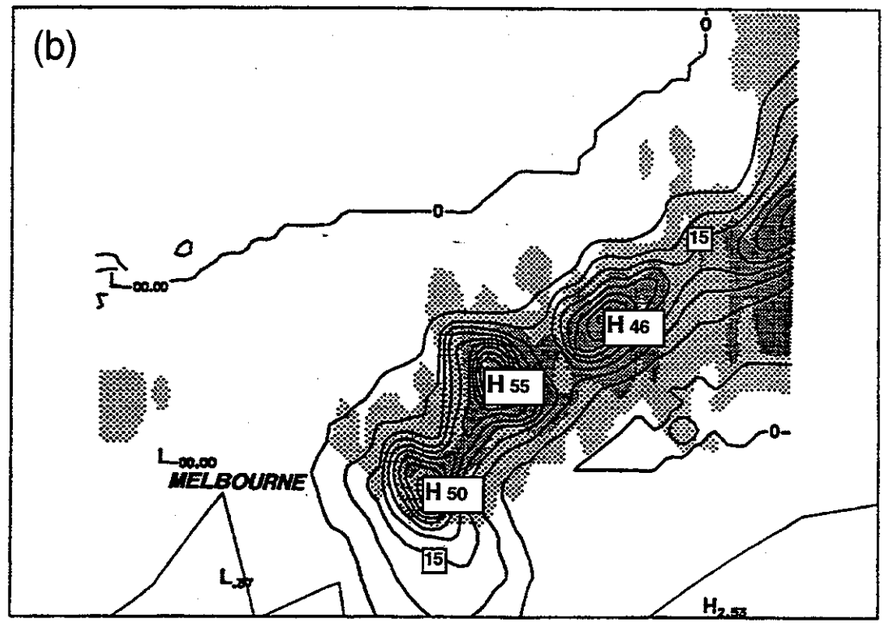

Figure 2: (a) The observed rainfall and associated orography for the 24-hour period between 0000 UTC 25/7/88 and 0000 UTC 26/7/88. Isohyet interval is 10 mm. The dashed box corresponds to the model domain shown in (b). (b) The model predicted accumulated rainfall for the 24-hour period from 0000 UTC on 25/7/88 to 0000 UTC on 26/7/88. Isohyet interval is 5 mm.

3. Southeastern Australian Storms

This Section shows that extreme storms, representative of the GSAM, can be simulated using a mesoscale atmospheric model. The events chosen for this study are the east coast low of 5 to 8 August, 1986 and the upper-level cut-off low of 28 April to 1 May, 1988. Both of these events caused significant spill from the Warragamba Dam (Dodds, 1997 - private communication). See Figure 3 for locations mentioned in the text.

East coast lows have been identified as the major cause of flood-producing rains on the east coast of Australia. These intense extratropical cyclones are characterised by heavy rainfall and strong winds, often of tropical cyclone strength. Holland *et al.* (1987) identified three types of east coast lows that occur typically in autumn or winter with an average frequency of one or two per year. Because east coast lows are generally of sub-synoptic scale and develop rapidly, they are difficult to forecast and operational quantitative prediction forecasts have been poor. Leslie *et al.* (1987) investigated the predictability of east coast lows and showed that the initial development of these systems could be forecast in a numerical model of 150 km horizontal resolution. However, they found that higher resolution is required to capture fully the intensity, structure and track of the system. In later studies, Hess (1990), McInnes and Hess (1992) and Golding and Leslie (1993) demonstrated the sensitivity of model results to improvements in both the model resolution and physical parameterisations.

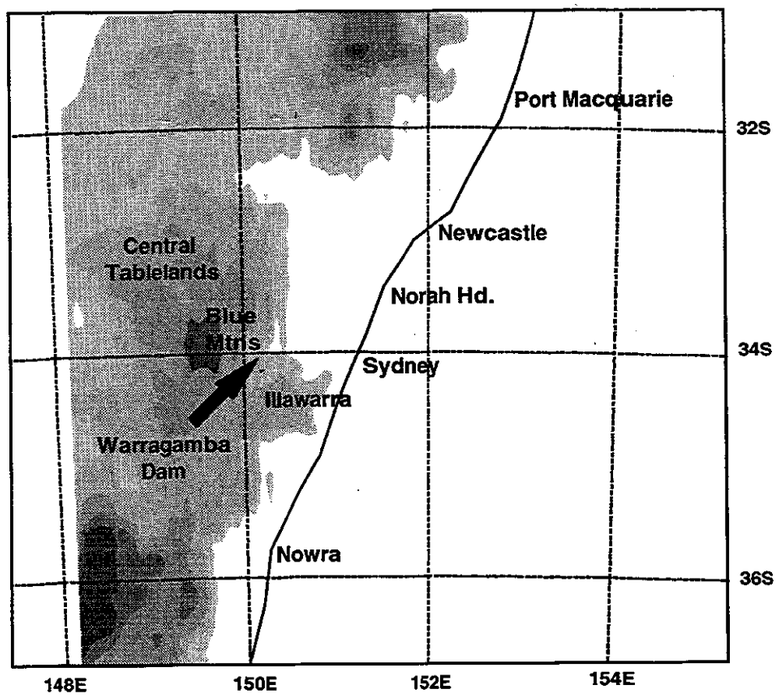

Figure 3: Map showing locations mentioned in the text. Shading indicates terrain above 250 m.

The meteorology of the formation and development of the east coast low of 5 to 8 August, 1986 has been described in detail by both Lynch (1987) and Bureau of Meteorology (1987). This east coast low produced the worst flooding to occur in Sydney for more than a century. The heavy rain extended to the Central Tablelands and Illawarra districts and caused major flooding of the principal river systems of the Sydney basin over this period. The Sydney rainfall for the 24 hours ending 9 am on 6 August was 328 mm. (Bureau of Meteorology, 1987), with the most intense phase of the rainfall occurring on 5 August. The rainfall was associated with a low-pressure system that had formed off the coast near Port Macquarie during the evening of the 4th, then moved SSW to near Norah Head by 0900 on the 5th. The low remained in this approximate area for the next 18 hours. Intensity-frequency-duration curves for Sydney Central showed that, for short durations, the intensities were not exceptional but that, for durations beyond 8 hours, the average intensity exceeded the 1 in 100-year event (Bureau of Meteorology, 1987).

A second type of cut-off low is referred to by forecasters as an "upper-level cut-off low". These systems have a closed circulation at the 500 hPa level but there is no manifestation at the surface. They are usually associated with intense thunderstorm activity rather than the large scale stratiform rain and strong winds that occur with east coast lows (McInnes *et al.*, 1992). The upper-level cut-off low of 28 April to 1 May, 1988 produced heavy rainfall along the coast and Illawarra escarpment to the south of Sydney. The rainfall was much lighter in the Blue Mountains, west of Sydney. The most intense phase of the storm occurred in the 24 hours ending at 0000 UTC on 30 April. The rainfall was associated with an upper-level cut-off low which was evident at 700 hPa from 0000 UTC on 27 April until 1200 UTC 30 April. After this, the weakened and moved eastwards away from the coastline.

3.1 Model Initialisation

In the simulations discussed here, the numerical model has been initialised using European Centre for Medium-Range Weather Forecasts (ECMWF) analyses that are available at a resolution of 2.5 degrees latitude and longitude for the entire globe. These analyses have been interpolated horizontally and vertically to the coarsest mesh; they also provide the temporal forcing on the lateral boundaries of the coarsest mesh. Three levels of interactive grid nesting were used, the coarsest having a horizontal grid spacing of approximately 60 km and the finest having a grid spacing of approximately 7 km. Ideally, higher resolution would have been desirable, but computing constraints made this difficult to achieve.

The terrain used on all meshes was interpolated from a 1/40th degree data set. The sea surface temperatures (SST) were obtained from the ECMWF analyses and enhanced in the waters off New South Wales with data from the weekly SST analyses of the Royal Australian Navy. In these simulations the microphysics parameterisation was activated on all grids. In addition to the microphysics scheme, the convective parameterisation scheme developed by Frank and Cohen (1985, 1987) was used on the two finest meshes. Companion simulations made as part of our study showed that in both cases it was necessary to use a convective parameterisation scheme on the finest grid to initiate convective development in locations close to those observed. In these simulations the convective scheme is phased out as the convection matures.

3.2 1986 East Coast Low: 4-6 August

3.2.1 Validation

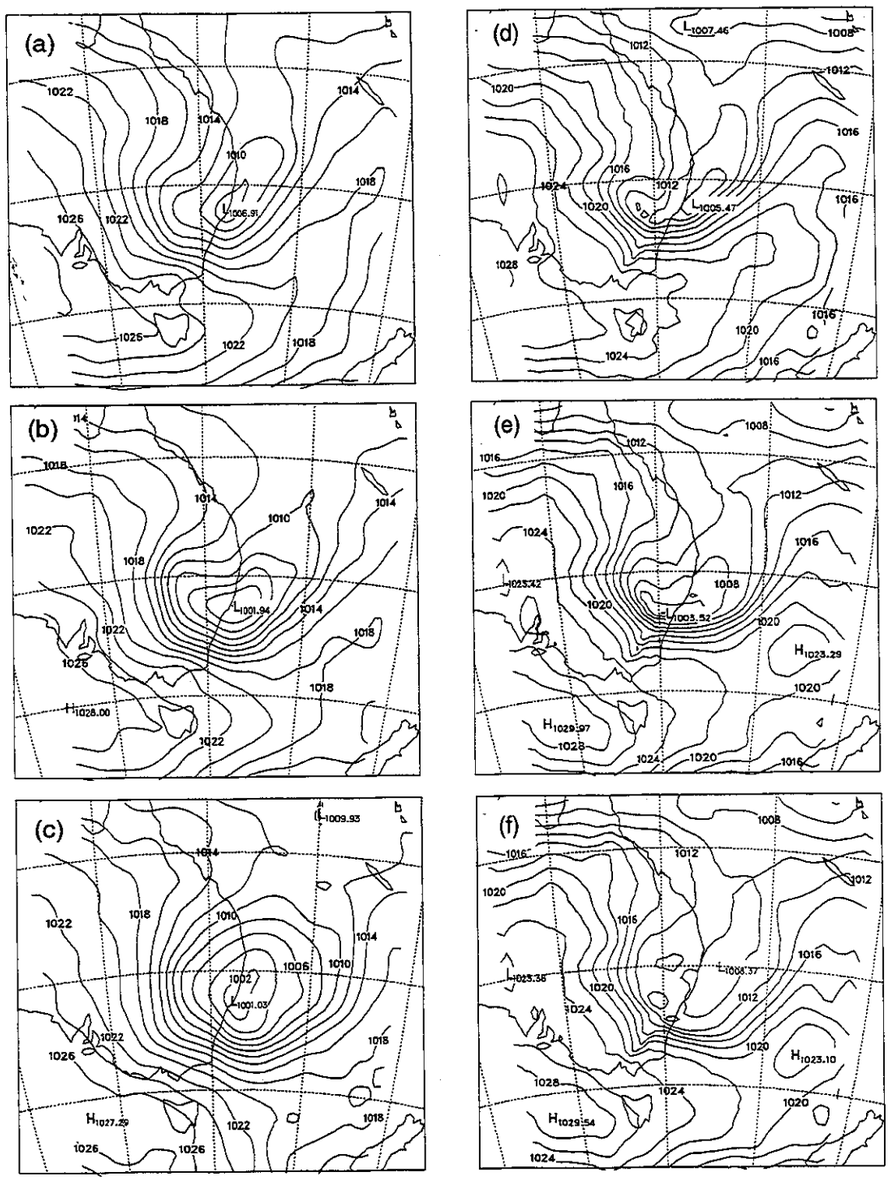

Figure 4: Mean-sea-level pressures (hPa) from the ECMWF analyses for (a) 0000 UTC, 5 August, (b) 1200 UTC, 5 August and (c) 0000 UTC, 6 August and model predicted mean-sea-level pressures for (d) 0000 UTC, 5 August, (e) 1200 UTC, 5 August and (f) 0000 UTC, 6 August.

For the east coast low study, the model simulation commenced at 1200 UTC on 4 August and was run for the next 36 hours, finishing at 0000 UTC 6 August. Figure 4 compares the ECMWF mean-sea-level pressure analyses with the mean-sea-level pressures predicted by the model for 0000 UTC and 1200 UTC on the 5th and 0000 UTC on the 6th. The main feature to note is the rapid decrease in central pressure of the low between 0000 and 1200 UTC and the close agreement between the modelled and ECMWF pressures. The predicted pressure also agrees with the observed central pressure of the low as presented in Figure 13 of Bureau of Meteorology (1987). At both of these times the modelled pressures are within 1 hPa of both the ECMWF and observed pressures. At 0000 UTC on the 6th there is less agreement between the model and ECMWF analyses, with the model beginning to increase the central pressure of the low and the ECMWF analyses indicating little change in the central pressure of the low. It is believed that this erroneous pressure rise is related to the prediction of the convection on the finest mesh, as the rise does not occur in simulations with two levels of grid nesting. Throughout the 24-hour period shown here there has been little horizontal movement of the low.

Figure 5 compares the wind field at the lowest model level (50 m) and mean-sea-level pressure at 0500 UTC, 5 August with observations. The features to note are the strong convergence of the low level winds at the leading edge (i.e. south of the centre) of the low and the weak winds that occur inland and north of the low centre. At this time the modelled central pressure of 1003 hPa compares favourably with the observed of 1002 hPa. The main difference between the model predicted and observed fields is that the model positions the low approximately 60 km further north and possibly slightly further offshore than observed.

These discrepancies in the position of the low are reflected in the precipitation predicted by the model. Figure 6 shows the 24-hour precipitation, ending at 2300 UTC on the 5th, for both the model prediction and the observed. Both the model and observations show a band of heavy precipitation, of approximately 300 mm, extending inland to the Blue Mountains. The major difference between the two fields is that the model predicts the band of heavy rainfall to occur further north than observed. In addition, the northern boundary of the rainfall band occurs further north in the model prediction. The orographic effect of both the Blue Mountains and the Illawarra escarpment is obvious in the local maxima in the precipitation over both of these regions. As in the observations (Bureau of Meteorology, 1987) the maximum rainfall lies to the west of the Illawarra escarpment and along the southern escarpment of the Blue Mountains. The predicted rainfall amounts over both the Blue Mountains and the Illawarra escarpment are very close to those observed. Intensity-frequency-duration curves (not shown) have been calculated for this simulation. These indicate that the model has been able to capture the extreme intensity of the 8-hour duration precipitation.

When considering the quality of the model prediction it must be kept in mind that these predictions have been produced at a horizontal resolution of approximately 7 km from initial conditions that are available at a resolution of approximately 250 km. Overall the model has predicted a realistic development of the east coast low and the predicted precipitation amounts and intensities are close to the extreme values observed. Consequently, we believe that this simulation provides an adequate test for many of the assumptions made in the estimation of PMP values.

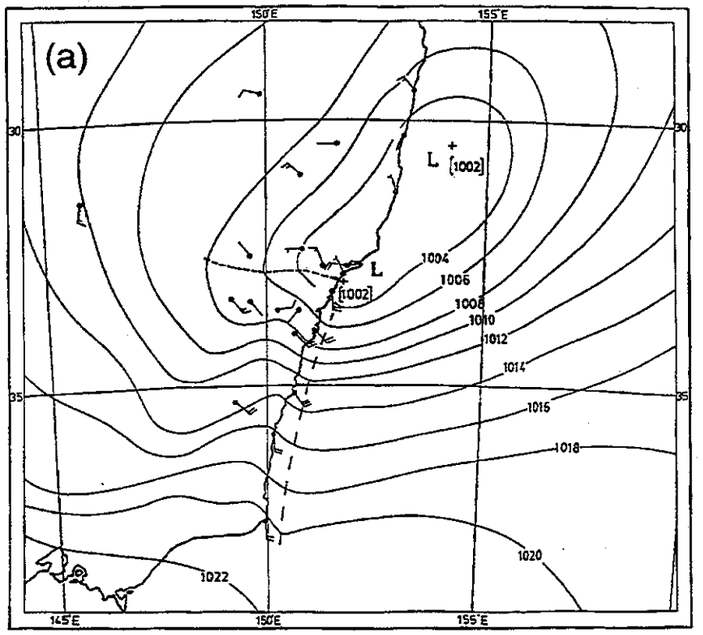

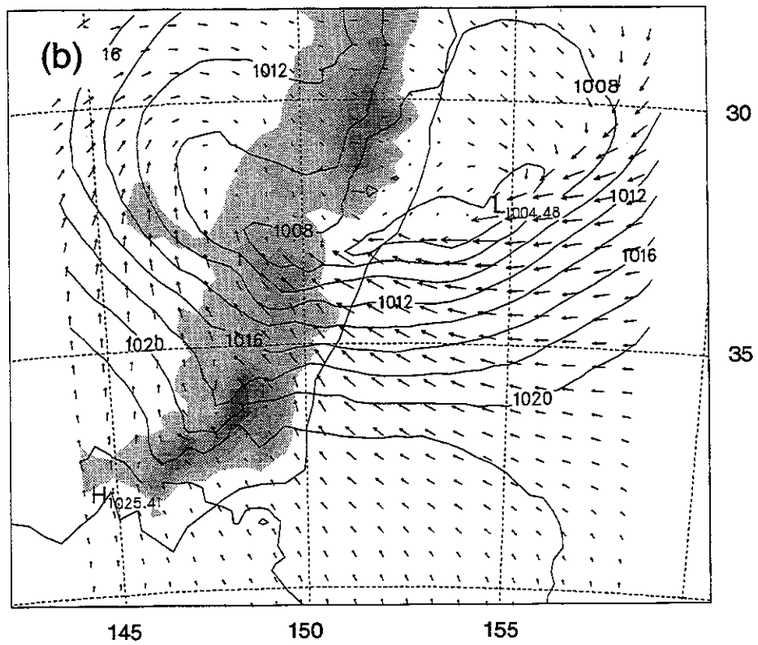

Figure 5: (a) Observed regional mean-sea-level pressure analysis (hPa) at 0500 UTC, 5 August (from Bureau of Meteorology, 1987) and (b) simulated regional mean-sea-level pressure analysis (hPa) at 0500 UTC, 5 August. Shading indicates terrain higher than 250 m.

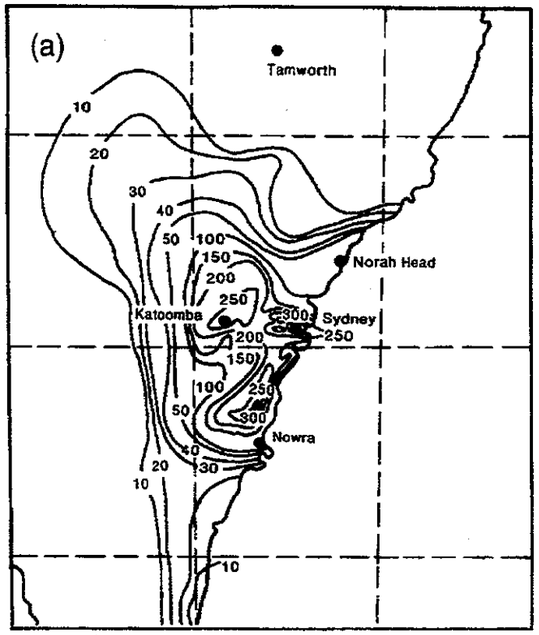

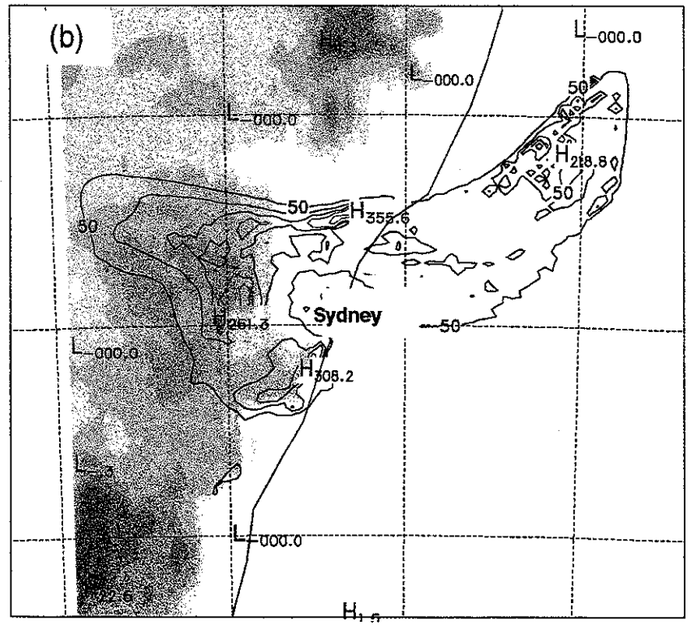

Figure 6: (a) Observed rainfall (mm) for the 24 hours ending 2300 UTC, 5 August (from Bureau of Meteorology, 1987) and (b) simulated rainfall (mm) for the 24 hours ending 2300 UTC, 5 August. Black contours are from 50 to 150 mm with a contour interval of 50 mm. Red contours are for rainfalls greater than 200 mm and have a contour interval of 100 mm. Shading indicates terrain higher than 250 m.

3.2.2 Increased Moisture Simulations

The simulations discussed in this section have been performed by initialising the model from the ECMWF analyses as before, but in this case the moisture values have been increased by uniformly increasing the temperatures of the atmosphere everywhere, while maintaining the relative humidities. In this way the system is still in dynamic balance but the specific humidity, and hence precipitable water, has been increased. The maximisation factor is defined as the ratio of the precipitable water for the increased moisture simulation to the precipitable water for the control simulation. The maximisation factor is determined for those portions of the storm for which the atmosphere is saturated. This method is comparable to the technique used to maximise storms in the current approach.

Two simulations with higher moisture values have been performed; the first where the temperatures have been increased by 3 and the second where they have been increased by 5°C. Henceforth, these simulations will be referred to as EC86_3 and EC86_5 respectively.

Under both sets of conditions the development of the east coast low proceeded in a similar manner to that of the control simulation. The main differences related to the intensity of the low, which in these cases experienced a deepening of the central pressure of 3 hPa and 4 hPa, respectively, more than that of the control simulation. The position of the low is similar in both cases.

The precipitation predicted by the model for these two simulations is presented in Figure 7. The distribution of the precipitation for both cases is similar to that of the control simulation but the amounts are greater, particularly in the regions of maximum rainfall which occurred along the Illawarra escarpment, the Blue Mountains and the mesoscale convergence line. However, the results from EC86_5 show less rainfall produced in these three regions compared with the rainfall produced in EC86_3, however, a larger area is affected by precipitation. Hence the precipitation is not linearly related to the precipitable water.

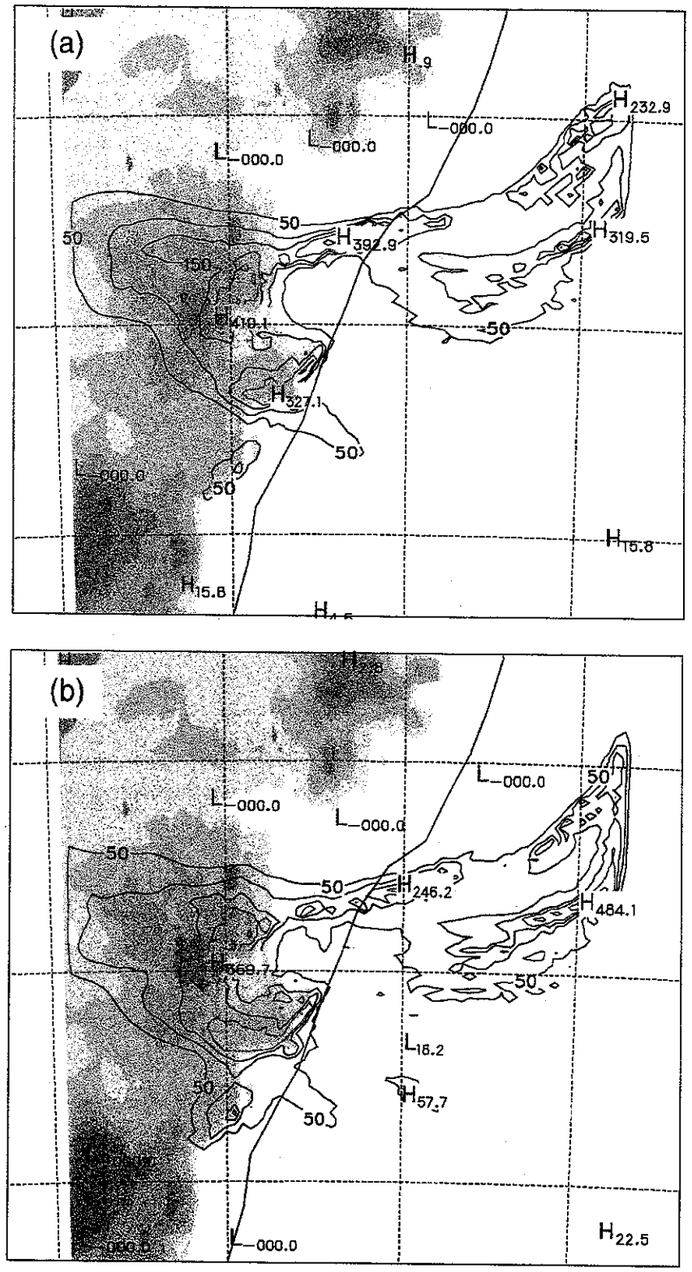

Figure 7: The predicted precipitation for the 24 hours ending 2300 UTC, 5 August for (a) EC86_3 and (b) EC86_5. Shading indicates terrain higher than 250 m. Contours are as for Figure 6(b).

3.2.3 Storm Efficiencies

In calculating the PMP for extreme storms, it is assumed that the precipitation efficiency of the storms is maximised. In this Section we will calculate the precipitation efficiency using output from the numerical model. The definition of precipitation efficiency is defined below and average efficiencies calculated for both the heavy and moderate rainfall regions of the storm.

Firstly, the modelled storm will be partitioned into heavy and moderate rainfall regions based on the method of Churchill and Houze (1984) and Tao *et al.* (1993). Model grid points with a rainfall rate in excess of 25 mm h^{-1} are considered to be heavy rainfall grid points. Precipitation at all other grid points is considered to be moderate rainfall. These definitions of heavy and moderate rainfall will be used throughout the remainder of this report.

The moisture and condensate mixing ratio continuity equations used in RAMS are given by

$$\frac{\partial r_n}{\partial t} = -u\frac{\partial r_n}{\partial x} - v\frac{\partial r_n}{\partial y} - w\frac{\partial r_n}{\partial z} + DIF(r_n) + \left(\frac{\partial r_n}{\partial t}\right)_{con} + \left(\frac{\partial r_n}{\partial t}\right)_{res} \qquad (6)$$

where r_n is the mixing ratio of individual condensate species (i.e. cloud water, rain, cloud ice, snow and aggregates). The first three terms on the right hand side of (6) are the advection of each condensate category, the fourth term denotes the diffusion of each condensate category and the subscripts *con* and *res* denote the tendency from the convective parameterisation and the resolvable scale microphysical parameterisation.

By summing (6) for each condensate species, neglecting diffusion and multiplying through by the density $\overline{\rho}$, the total condensate equation becomes

$$\overline{\rho}\frac{\partial r_t}{\partial t} = -\overline{\rho}u\frac{\partial r_t}{\partial x} - \overline{\rho}v\frac{\partial r_t}{\partial y} - \overline{\rho}w\frac{\partial r_t}{\partial z} + \overline{\rho}\left[\left(\frac{\partial r_t}{\partial t}\right)_{con} + \left(\frac{\partial r_t}{\partial t}\right)_{res}\right]. \qquad (7)$$

Vertical integration of (7) gives

$$\int_{sfc}^{z_t}\overline{\rho}\frac{\partial r_t}{\partial t}\Delta z = \int_{sfc}^{z_t} -\overline{\rho}u\frac{\partial r_t}{\partial x}\Delta z - \int_{sfc}^{z_t}\overline{\rho}v\frac{\partial r_t}{\partial y}\Delta z - P_0 + \int_{sfc}^{z_t}\overline{\rho}\left[\left(\frac{\partial r_t}{\partial t}\right)_{con} + \left(\frac{\partial r_t}{\partial t}\right)_{res}\right]\Delta z \qquad (8)$$

where P_0 is the surface precipitation rate. Equation (8) can be further integrated over the heavy and moderate rainfall regions.

The precipitation efficiency is defined as the ratio of the rainfall to the total condensation,

$$PE_c = \frac{P_0}{\int_{sfc}^{z_t}\overline{\rho}\left[\left(\frac{\partial r_t}{\partial t}\right)_{con} + \left(\frac{\partial r_t}{\partial t}\right)_{res}\right]\Delta z}. \qquad (9)$$

A similar definition of precipitation efficiency has been adopted in other modelling studies (Ferrier *et al.*, 1996; Weisman and Klemp, 1982).

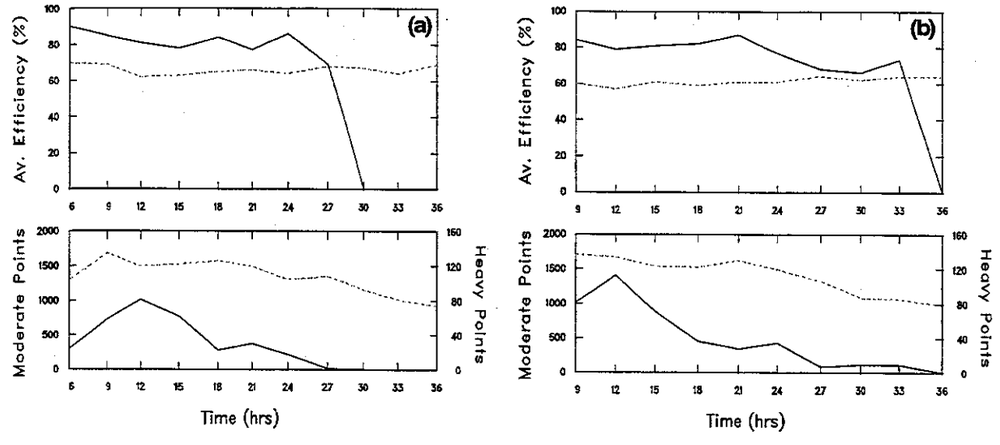

Figure 8: Plots of PE_c for the heavy (solid curve) and moderate (dashed curve) portions of (a) the control simulation, (b) EC86_3 and (c) EC86_5. The lower panel shows the number of heavy (solid) and moderate (dashed) rainfall grid points on the finest mesh.

The temporal variation of PE_c for both the heavy and moderate rainfall portions of the system, is shown in Figure 8. In all cases the system is 60-70% efficient at generating moderate rainfall. For the case of the heavy rainfall, the production of precipitation is 80-90% efficient.

As the amount of moisture available to the system increases, there is a tendency for PE_c to decrease for moderate rainfall. The lower panels of Figure 8 show that as the moisture available to the system is increased the number of heavy rainfall grid points increases and the heavy rainfall is longer lived.

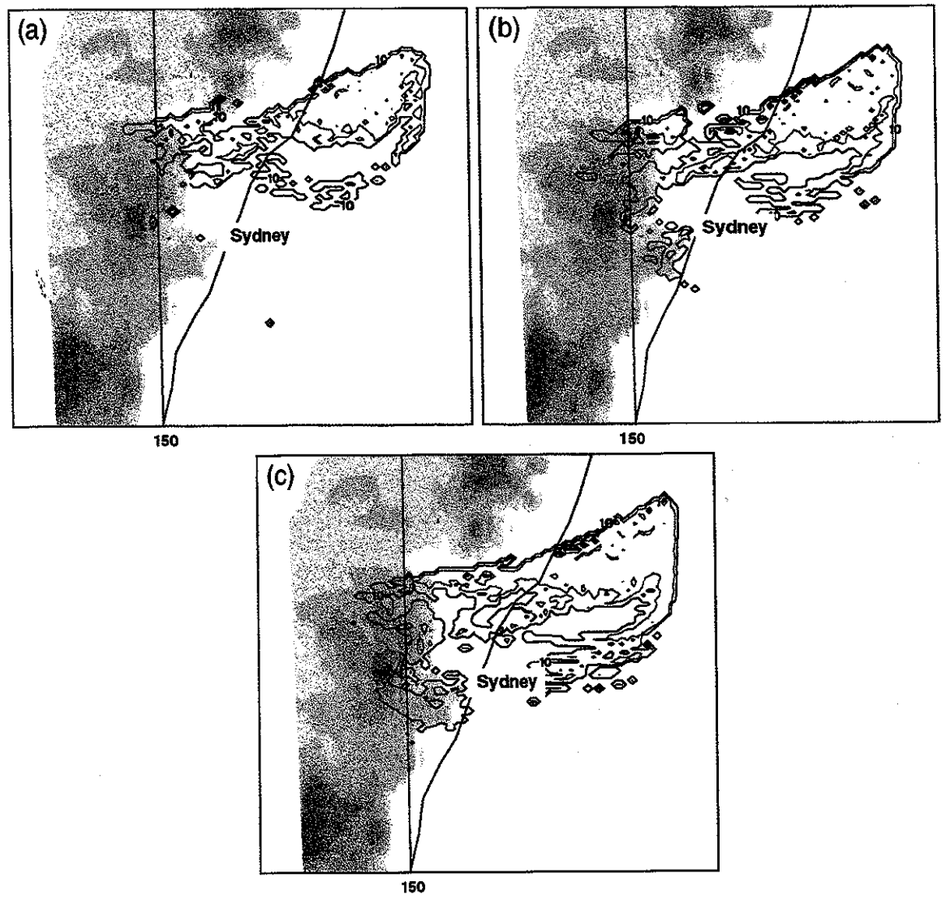

Figure 9: Plots of the percentage of the total rainfall which falls as heavy rainfall (i.e. with a rainfall rate greater than 25 mm hr^{-1}) for (a) the control simulation, (b) EC86_3 and (c) EC86_5. Black contours are for 10% and red contours are for 50 and 90%.

These statistics suggest that the percentage of the total rainfall that occurs as heavy rainfall may be important. This quantity has been calculated for the control simulation, EC86_3 and EC86_5 and plots of it are shown in Figure 9. For each simulation, the rainfall that falls in the main cloud band over the sea occurs as heavy rainfall. Over the land only a small percentage falls as heavy rainfall but this amount increases as the moisture availability increases. Figure 8 and Figure 9 indicate that long-lived moderate rain processes are important and that the efficiency of these processes may decrease as the moisture availability increases. On the other hand, this may be offset by increases in the percentage of rain falling as heavy rainfall.

3.2.4 Terrain Effects

When estimating PMP values for a particular storm it is usual to attempt to separate out the convergence and topographic components of the storm. The concept underlying this technique is that the convergence component is due to synoptic-scale atmospheric disturbances such as frontal lifting. The portion of the rainfall that cannot be separated into the convergence component is defined as the topographic component of the storm.

In this section results are presented for a simulation without terrain. This simulation may be considered to be the model equivalent of the convergence component for this storm. The convergence component rainfall is then subtracted from the rainfall of the control simulation to provide an estimate of a model-derived topographic component of this storm. The convergence and topographic components of the storm are presented in Figure 10.

These results show that over the Blue Mountains and Illawarra escarpment all of the rainfall is due to the topographic component of the storm. However, along the convergence line, the results are more complicated. The removal of terrain has allowed the entire system to move south faster than in the case of the control simulation. Consequently, the rainfall maximum of 267 mm, for the "no terrain case", occurs further south than the corresponding maximum of 355 mm for the control simulation. The effect of this difference may be seen in the adjacent, large maximum and minimum values of Figure 10(b). A topographic component of approximately 100 mm in this region is more realistic. However, these results illustrate that terrain effects do feed back to synoptic-scale aspects of the storm.

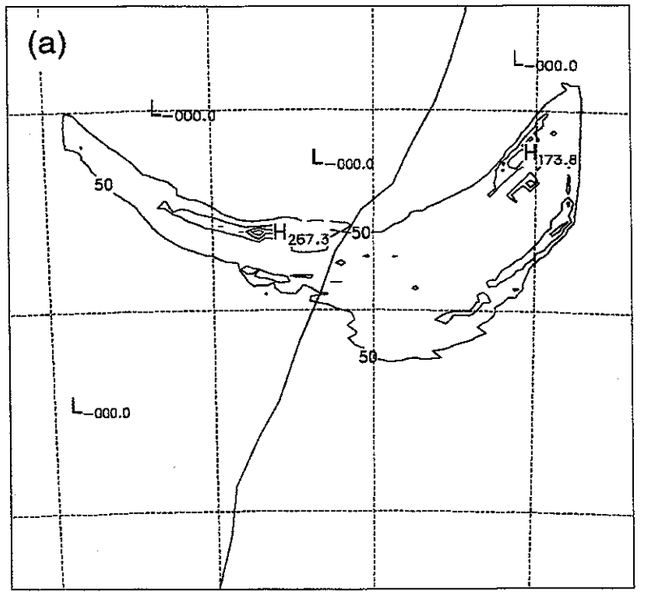

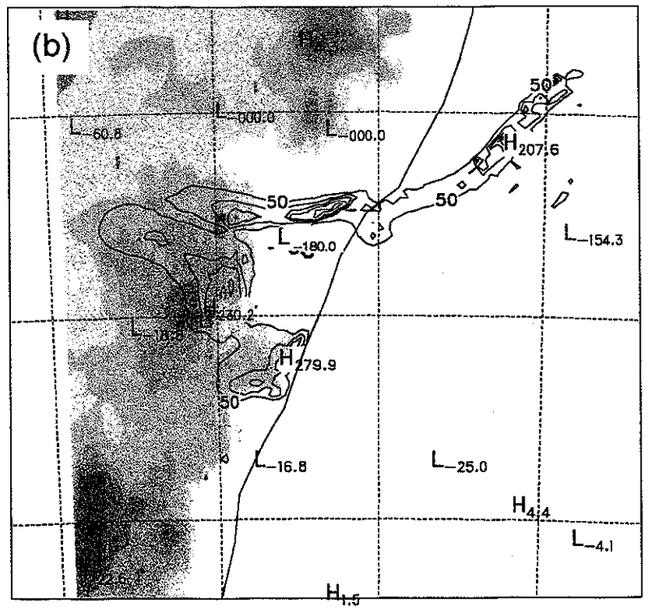

Figure 10: The (a) convergence and (b) topographic components of the storm. Contours as for Figure 6(b).

3.2.5 Temporal Variation of Precipitation

The temporal variation of the precipitation (Figure 11) for the control simulation indicates an association between the rainfall intensity and the movement and deepening of the low. The maximum rainfall rates along the "convergence line" are associated with the rapid deepening of the low between 0000 UTC and 1200 UTC (12 and 24 hours of simulation) on the 5th. As the central pressures associated with the low begin to increase and the low moves southward, the heavy rainfall ceases.

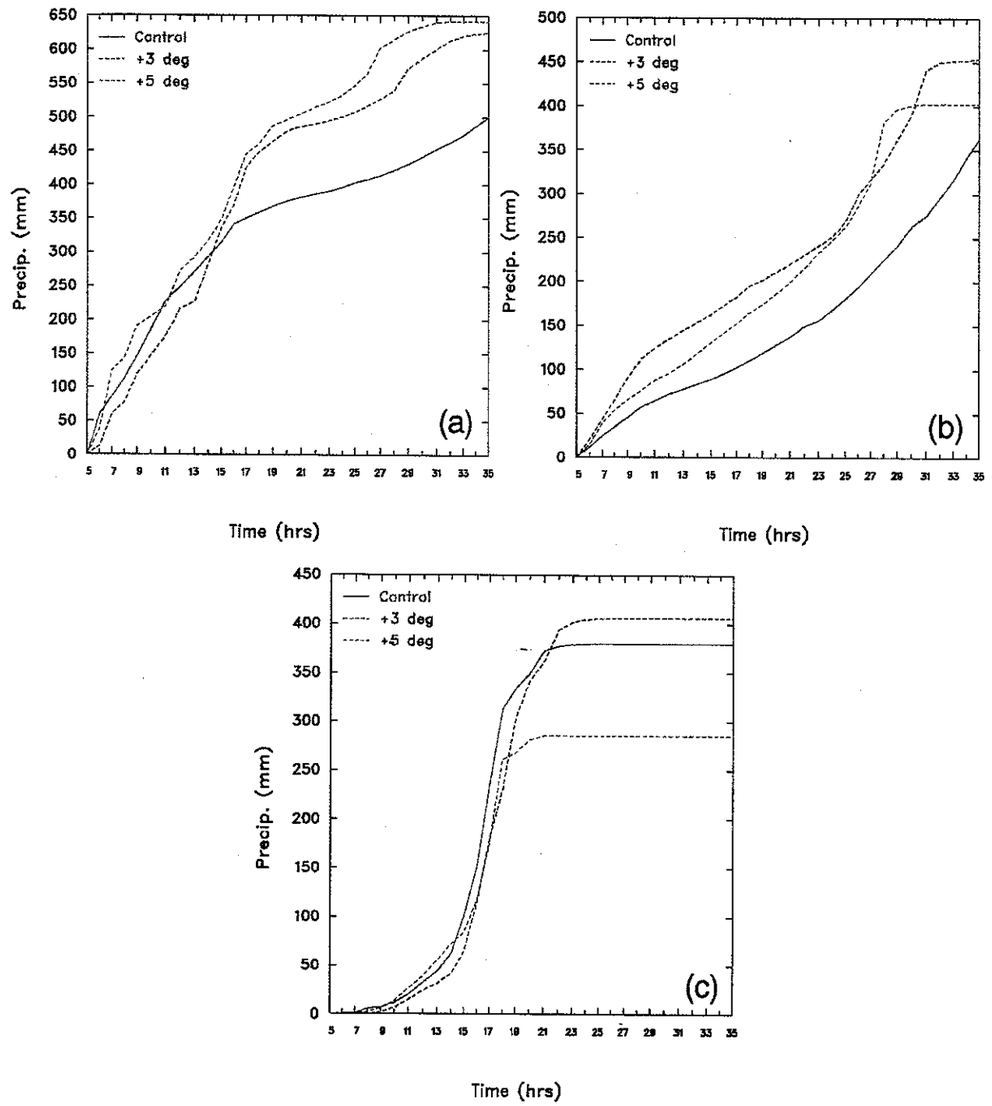

Figure 11: Time series of precipitation representative of (a) the Blue Mountains, (b) the Illawarra escarpment and (c) the convergence line for the control simulation, EC86_3 and E86_5

Bureau of Meteorology (1987) notes the greater temporal variation in the observed rainfall rate in the Blue Mountains. Similarly, greater variation is noticeable in the simulated rainfall rates for the Blue Mountains. At this location, orographic effects act to increase the low level convergence. In contrast, the rainfall rates over the Illawarra escarpment are relatively constant (both modelled and observed) implying that here the orographic component dominated.

Similar variation is noted for EC86_3 and EC86_5. The temporal variation of the precipitation for these simulations also illustrates that changes in the moisture field feeds back to the dynamics by affecting both the intensity and movement of the low. This is particularly noticeable over the Illawarra escarpment, where changes in the movement of the low act to decrease the component of the wind normal to the escarpment earlier, compared with the control simulation. This results in the rainfall for EC86_3 and EC86_5 ceasing earlier than it does for the control simulation.

3.2.6 Depth-Duration-Area Analysis

The model-derived precipitation fields have been used to calculate Depth-Duration-Area curves for the control simulation, EC86_3 and EC86_5. These curves are based on hourly rainfall rates for the finest mesh simulated, and calculated using the same method as Minty *et al.* (1996). This method differs slightly from the standard method (WMO, 1969) in that multi-centred storms are treated as if they were single centred. *"The program which determines the maximum depth-area curve for each storm simply counts the number of grid points in between evenly incremented isohyets, from the maximum to the minimum isohyet, and calculates the arithmetic mean rainfall per interval. Area calculations are based upon the number of grid points counted and the known resolution of the grid."* (Minty *et al.*, 1996).

In all cases, the hourly rainfalls used in these analyses are from 6 hours of simulation to the completion of the simulation. Depth-area curves are calculated for the standard durations of 2, 12, 24, 36 and 48 hours.

Depth-area curves, for durations of 2 hours and 24 hours, are shown in Figure 12 for the control simulation, EC86_3 and EC86_5. Also shown is the "observed" curve for this storm for a duration of 24 hours. A comparison of the observed and control curves shows that the model is producing high rainfall amounts for small areas. The reason for this discrepancy is unknown, but it may be associated with the inability of the model to adequately resolve features even at the relatively high resolution used in this work. For areas greater than 1000 km^2 there is good agreement between the two curves.

The depth-area curves for EC86_3 and EC86_5 show greater rainfall depths for all areas and for durations of 2 hours and 24 hours. The maximisation factors associated with these simulations are 1.15 and 1.3 respectively. These values are much lower than the maximisation factor of 1.8 used by the Bureau of Meteorology to maximise this storm (Minty, 1997 - private communication). For both cases the maximised curves (derived by applying equation (5)) lie below the corresponding, simulated depth-area curve. This indicates that for durations of 2 and 24 hours, the current maximisation method is under-estimating the precipitation for all

areas. For this case study the model produces between 15% and 25% more precipitation than the maximisation relationship of the current PMP technique for areas of 50 to 70 km^2. For areas of 500 km^2, the model produces between 5% and 15% more precipitation than the maximisation relationship of the current PMP technique. Hence the precipitation is not linearly related to the precipitable water.

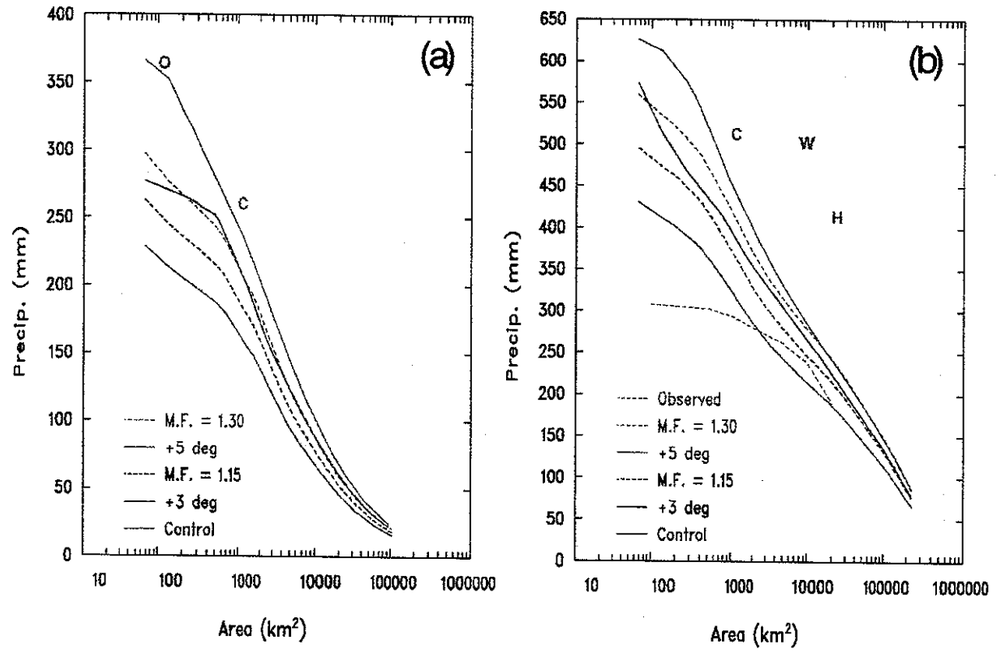

Figure 12: Depth-area curves for (a) 2 hours and (b) 24 hours for the control simulation (solid, red curve), EC86_3 (solid, blue curve) and EC86_5 (solid, green curve). Also shown are curves corresponding to maximisation factors of 1.15 (dashed, blue curve) and 1.3 (dashed, green curve). The observed depth-area curve (dashed, orange curve) for a duration of 24 hours is shown on (b). The letters O, C, W and H indicate the 2 and 24-hour PMP values for the catchments of the Oberon, Chifley and Warragamba Dams and the Hawkesbury-Nepean catchment, respectively.

The 2-hour PMP values for the Oberon and Chifley Dam catchments and the 24-hour PMP values for the catchments of the Chifley and Warragamba Dams and the Hawkesbury-Nepean catchment (Pearce *et al.*, 1992, 1993) have been included on Figure 12 for comparison. The 2-hour PMP values have been determined using the GSDM (Bureau of Meteorology, 1985). The 24-hour PMP values have been determined using the method outlined in Section 1.2. For both durations the model has been able simulate a small area storm approaching the PMP values for the Oberon and Chifley Dam catchments. For larger areas, the 24-hour PMP values for the Warragamba Dam and the Hawkesbury-Nepean catchments lies well above the depth-area curves for the east coast low of August 1986. This indicates that, for this particular storm, the model has not been able to be maximised to a level approaching a PMP storm. However, it may be possible to maximise other storms to the PMP values for larger areas.

3.3 1988 Upper-level cut-off low: 28-30 April

3.3.1 Validation

The simulation of the upper-level cut-off low commences at 0000 UTC on 28 April and runs for the next 60 hours, finishing at 1200 UTC 30 April.

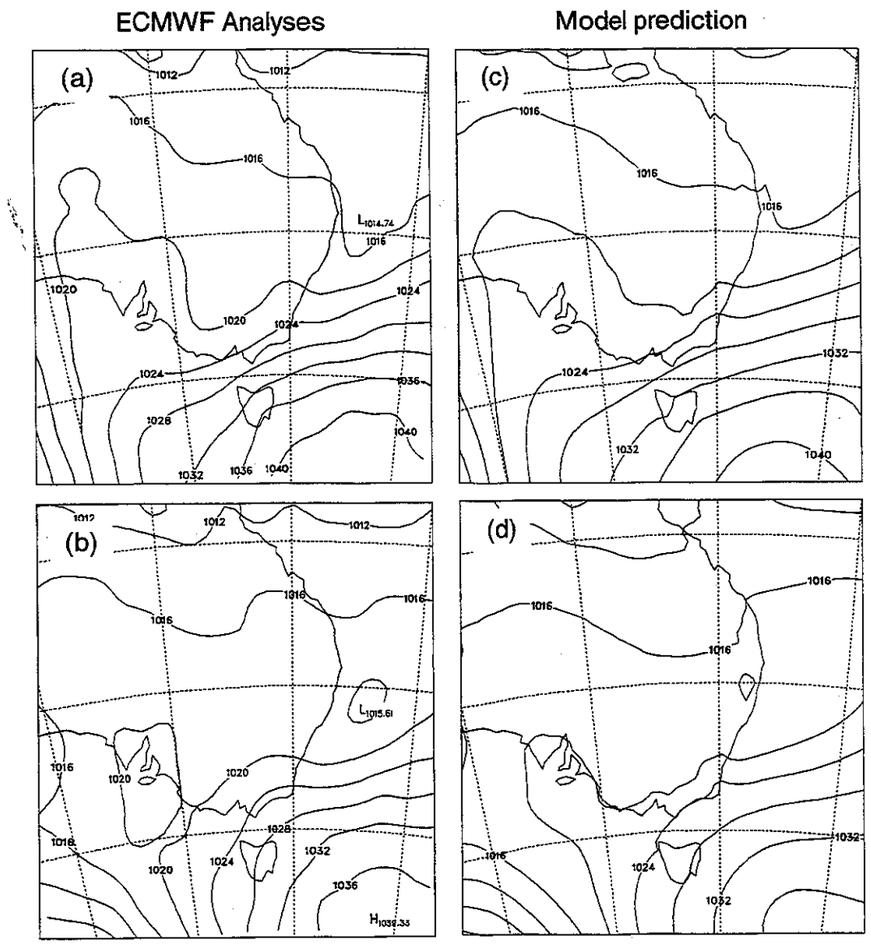

Figure 13: Mean-sea-level pressures from the ECMWF analyses for (a) 0000 UTC, 29 April and (b) 0000 UTC, 30 April, and model predicted mean-sea-level pressures for (c) 0000 UTC, 29 April and (d) 0000 UTC, 30 April.

The ECMWF mean-sea-level pressure analyses are compared with the mean-sea-level pressures predicted by the model for 0000 UTC on the 29th and the 30th (Figure 13). On the 29th the main features to note are the trough in the 1016 hPa isobar and the ridge extending to the northwest located along the southern Australian coastline. Both of these features are

predicted by the model. By the 30th the trough has developed into a mesoscale cut-off low. The evolution of this feature is also captured by the model, however, the model predicts the low to occur further west than represented in the ECMWF analyses.

The observed surface winds and the winds at the lowest model level corresponding to 0000 UTC on the 30th are shown in Figure 14. In both cases strong (15 ms^{-1}) easterly to east-southeasterly winds occur along the coastline south of 35°S. In the vicinity of Sydney the winds weaken and veer to have more of a southerly component. To the north the wind speeds are much lighter. Between approximately 33 and 35°S there is quite strong convergence of the winds along the coastline itself. It is this feature which acts to "focus" the region of high precipitation in this case.

The observed and predicted precipitation corresponding to the 24 hours ending 0000 UTC on 30 April are shown in Figure 15. In the simulation this corresponds to the precipitation predicted to occur between 24 and 48 hours of simulation. In both cases the features to note are the high rainfall amounts which occur along the coastline but are greatest in the vicinity of the Illawarra escarpment. Lighter rainfall amounts extend further inland but in this case there is less evidence of orographic enhancement. The second feature that the model has captured is the abrupt decrease in rainfall amount north of 33°S. The model has not captured the high rainfall amounts that were recorded in the Sydney basin. It is possible that one reason for this discrepancy is because the model is unable to resolve the complex orography of that region at a resolution of 7 km.

As in the previous case, the model has predicted a realistic development of the system and the predicted precipitation amounts and its spatial distribution are close to those observed. Consequently, we believe that this simulation also provides an adequate test for many of the assumptions made in the estimation of PMP values.

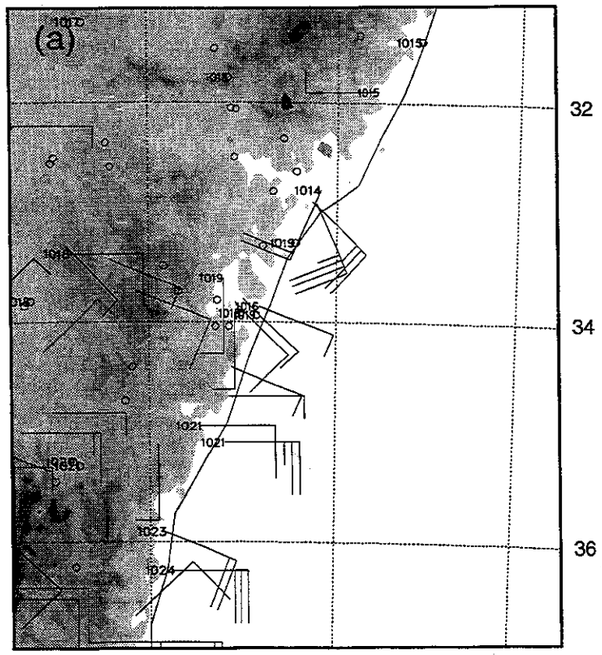

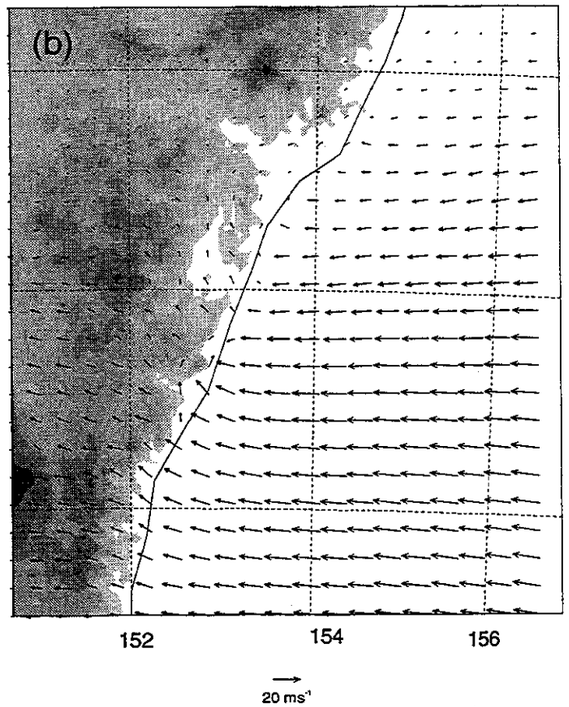

Figure 14: (a) Observed surface winds at 0000 UTC, 30 April. (b) Predicted winds at the lowest model level for 0000 UTC, 30 April. Shading indicates terrain higher than 100 m.

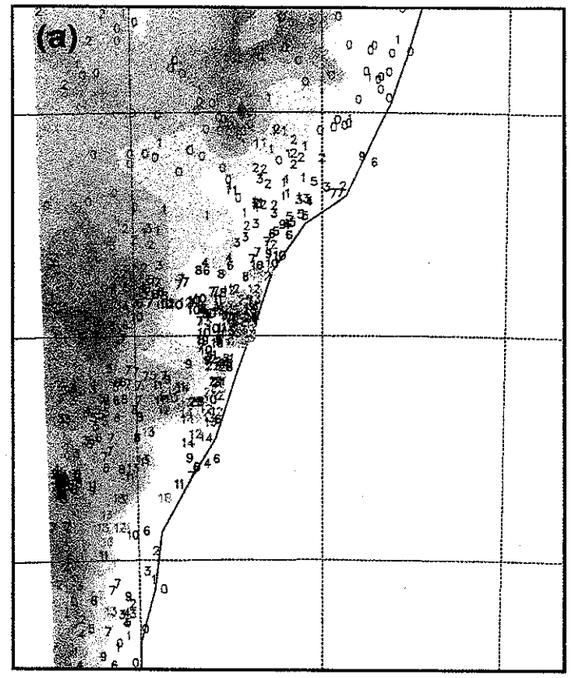

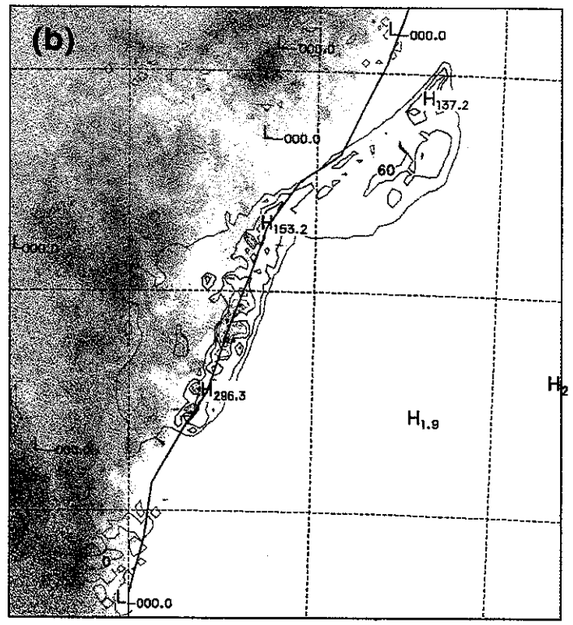

Figure 15: The (a) observed and (b) predicted precipitation for the 24 hours ending 0000 UTC, 30 April. The observed rainfall is colour-coded to correspond with the contours of Figure 15(b). Orange and red contours correspond with amounts greater than 180 mm. The Contour interval is 30 mm. Shading indicates terrain higher than 100 m.

3.3.2 Increased moisture simulations

The simulations discussed in this Section have been performed by initialising the model as described above in 3.2.2.

Simulations using a temperature increase of 3°C and 5°C were attempted, but for these cases the perturbation to the thermodynamic equation used by the model were no longer valid as the model produced unrealistic results (see Section 2.1(c)). Consequently, the simulation discussed in this section has been produced using a smaller temperature increase of 1.5°C. In addition, a simulation with a temperature decrease of 1.5°C was performed to determine if Equation (5) is valid. These simulations shall be referred to as UC88_P(lus) and UC88_M(inus) respectively.

The predicted precipitation for these two simulations is shown in Figure 16. The overall distribution of the precipitation is similar for these two simulations and the control simulation, with the maximum precipitation occurring along the coastline in all cases. In UC88_M the predicted maximum precipitation is less than that predicted in the control simulation, and for UC88_P the maximum precipitation is greater than that predicted in the control simulation.

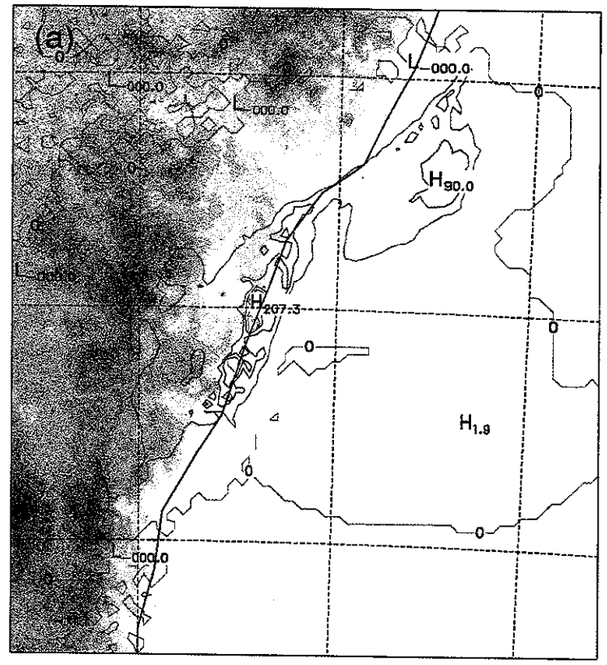

Figure 16 The predicted precipitation for the 24 hours ending 0000 UTC, 30 April for (a) UC88_M and (b) UC88_P. Contours as for Figure 15(b). Shading indicates terrain higher than 100 m.

3.3.3 Storm Efficiencies

Equation (9) has been used to calculate the precipitation efficiencies of the system for (a) the control simulation, (b) UC88_P and (c) UC88_M. As before, the hourly precipitation rate has been used to partition the storm into heavy and moderate rainfall regions. The temporal variation of PE_c is shown in Figure 17. For each simulation, the system is 60-80% efficient at generating moderate rainfall and 80-100% efficient at generating heavy rainfall. For these simulations there is little sensitivity of the precipitation efficiency to increases in the moisture available to the system.

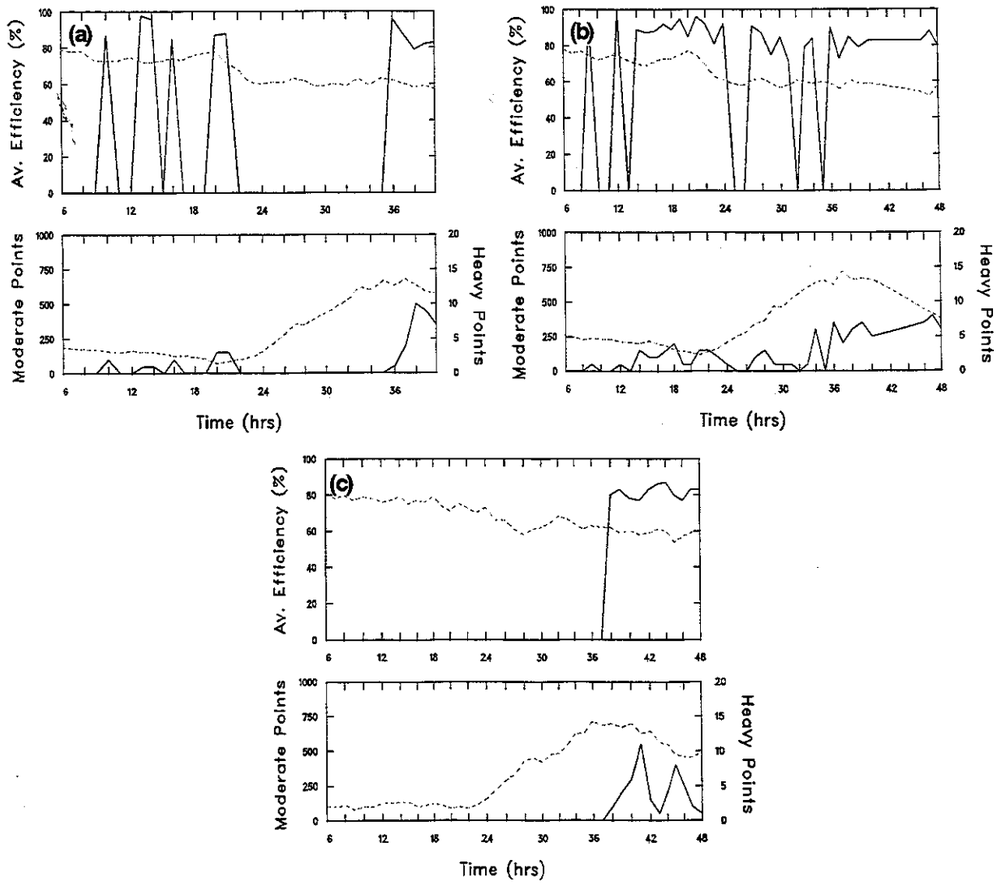

Figure 17: Plots of PE_c for the heavy (solid curve) and moderate (dashed curve) rainfall portions of (a) the control simulation, (b) UC88_P and (c) UC88_M. The lower panel shows the number of heavy rainfall (solid) and moderate rainfall (dashed) grid points on the finest mesh.

The lower panels of Figure 17 show that as the moisture available to the system is increased, heavy rainfall begins earlier and is more continuous. For all simulations, less than 10 grid

points may be considered to experience heavy rainfall. The percentage of the total rainfall that falls as heavy rainfall has been calculated for the 3 simulations (figures not shown). For the control and UC88_P this value was approximately 10% for the first 36 hours of the simulation and was confined to the high rainfall region along the coastline. From 36 to 60 hours of simulation this percentage increased to more than 50% in the high rainfall region along the coast. For the low moisture simulation (UC88_M) the amount of heavy rainfall was negligible.

3.3.4 Terrain Effects

In this Section, results are presented for a simulation in which the effects of terrain have been removed. As in Section 3.2.4, the resulting rainfall from this simulation is subtracted from that of the control simulation to determine the model-derived topographic component of the storm. The convergence and topographic components of the storm are presented in Figure 18.

The high rainfall amounts along the coastline are due to the topographic component of the storm. The wind fields presented in Figure 14 show strong convergence of the winds in this region. Close inspection of these fields suggests that this convergence is the result of either blocking or channelling of the low-level winds by the terrain.

Relatively high rainfall is predicted to occur over the ocean, east of Newcastle, due to the convergence component of the storm. This maximum does not occur in the control simulation.

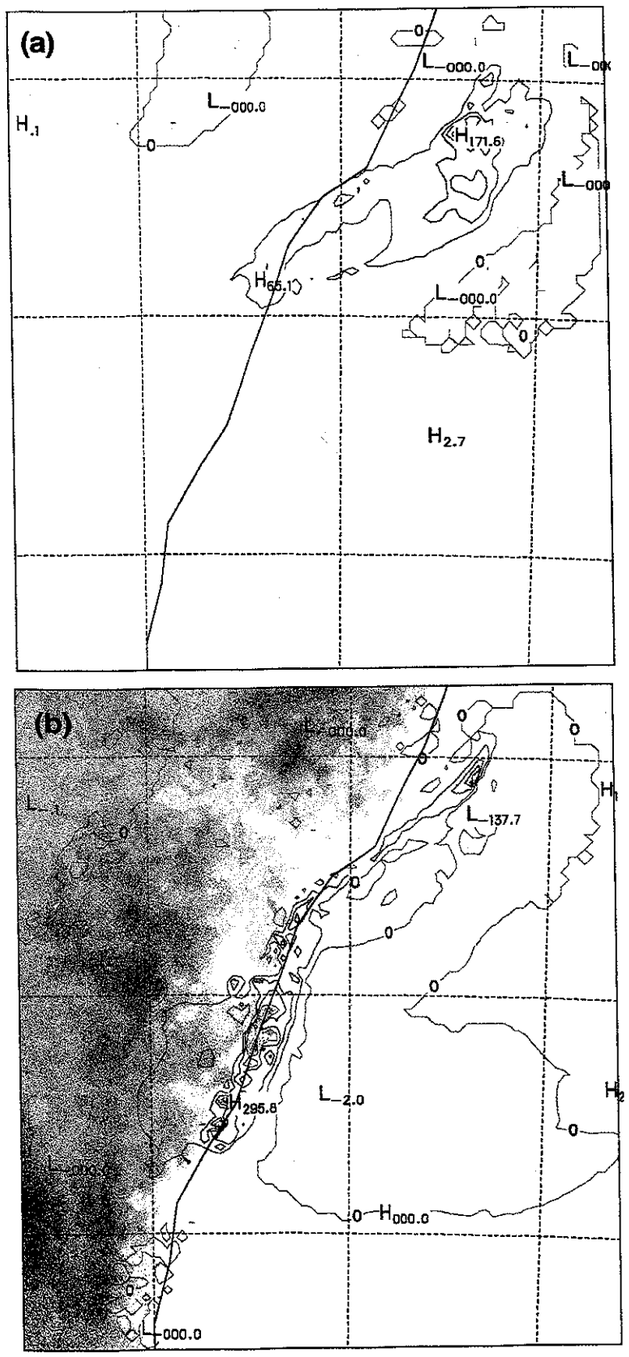

Figure 18: The (a) convergence and (b) topographic components of the storm. Contours as for Figure 15(b).

3.3.5 Temporal Variation of Precipitation

The temporal variation of the precipitation at 4 locations in the region of high rainfall is presented in
Figure 19. The control simulation is characterised by highly variable rainfall rates at each location throughout the 60 hours of simulation, indicating the growth and decay of individual convective cells. Features common to each location include an almost constant rainfall rate for the first 20 hours of simulation, followed by a period of almost negligible rainfall to 36 hours of simulation. The rainfall rates markedly increase after 36 hours and are both spatially and temporally variable.

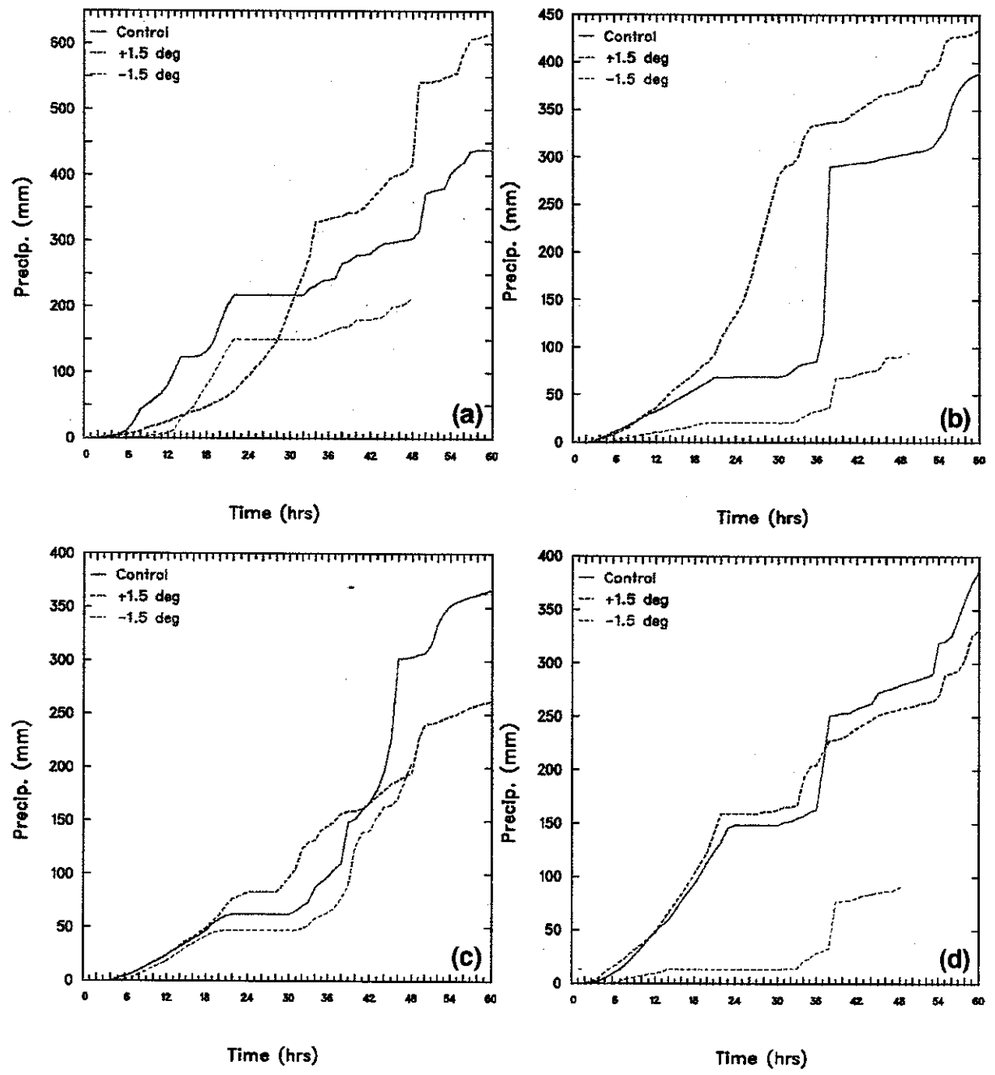

Figure 19: Temporal variation of the precipitation at 4 locations in the high rainfall region.

The low moisture simulation (UC88_M) has a similar variation in its precipitation time series. As expected, the rainfall rates are much lower for this simulation. The variation of the precipitation for the high moisture simulation (UC88_P) is also both spatially and temporally variable, but, in general, does not evolve in the same manner as the control or UC88_M.

3.3.6 Depth-Duration-Area Analysis

Depth-area curves have been calculated for standard durations of 2, 24, 36 and 48 hours (Figure 20). Simulation UC88_M did not proceed beyond 48 hours of simulation time, hence a depth-area curve for 48 hours is unavailable for this simulation.

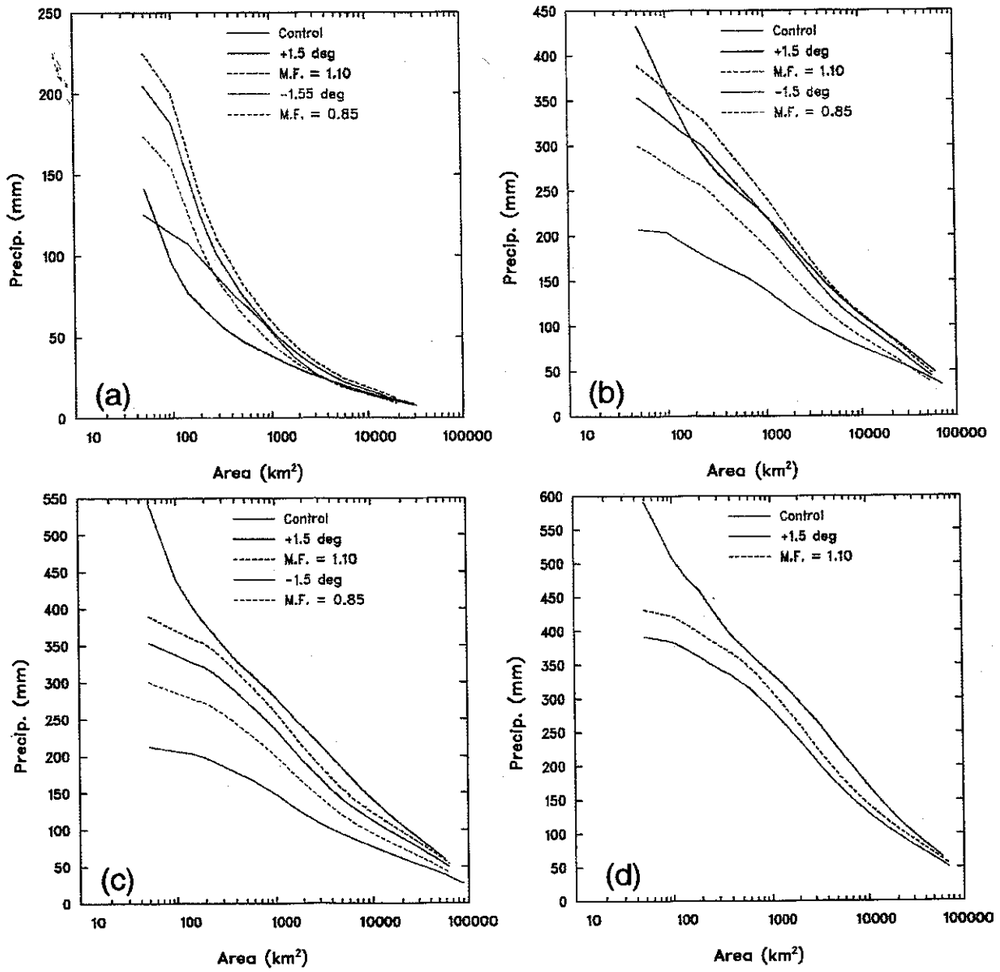

Figure 20: Depth-area curves for (a) 2 hours, (b) 24 hours, (c) 36 hours and (d) 48 hours for the control simulation (solid, red curve), UC88_P (solid, blue curve) and UC88_M (solid, green curve). Also shown are curves corresponding to maximisation factors of 1.1 (dashed, blue curve) and 0.85 (dashed, green curve).

For short durations (i.e. 2 hours) the rainfall depths of the control simulation are greater than those of both UC88_M and UC88_P. For durations of 36 and 48 hours the depth-area curve of the control simulation lies below that of UC88_P and above that of UC88_M. For UC88_P, the transition between these two situations occurs for durations of approximately 24 hours. For durations of 24 hours the curves corresponding to the control simulation and UC88_P are almost equal for areas greater than 200 km^2.

The maximised curves corresponding to a maximisation factor of 1.1 lie above the depth-area curve of UC88_P for durations of 2 and 24 hours. The reverse is true for durations of 36 and 48 hours. For these durations the current maximisation technique under-estimates the precipitation as predicted by UC88_P for all areas. For these cases, the model produces between 30% and 35% more precipitation than the current PMP technique for areas of 50 to 70 km^2. For areas of 500 km^2, the model produces between 5% and 10% more precipitation then the current PMP technique. For UC88_M, the current maximisation technique over-estimates the predicted precipitation. Hence the precipitation is not linearly related to the precipitable water.

3.4 Storm 3: The Dapto Flash Flood

A considerable amount of time was spent trying to simulate this important storm due to its importance to PMP studies. Shepherd and Colquhoun (1985) state "*A number of points, which are relevant to PMP studies, have been raised as a result of this storm. Estimates of PMP for short durations over rough terrain have since been revised upwards (Bureau Of Meteorology, 1984), because maximised depth-duration-area values during the event exceeded the adjusted U.S. data values in use at the time for a duration of six hours and areas less than about 220 sq km. The greatest difference was almost 160 mm for an area of 25 sq km. This event, other heavy rainstorms, and theoretical work cast doubt on the use of rough and smooth terrain categories for the purposes of estimating PMP for durations of less than 6 hours.*"

The meteorological conditions and features of this storm are well documented in Shepherd and Colquhoun (1985). A workshop paper (Abbs, 1993) was produced as a result of early work on this storm and is reproduced as Appendix A of the mid-project report (Abbs and Ryan, 1994). That paper summarises observations and results from a numerical simulation of the storm. Although the simulation is described as the "best attempt" to date, we are dissatisfied with this simulation and consider it to be unsuccessful. The main reasons behind this decision relate to the fact that the evolution of the modelled storm differs from observations, both in the meteorological characteristics of the storm and in the temporal variation of the rainfall.

Following Abbs (1993), experiments have continued in an effort to improve the simulation. These experiments have included simulations which have looked at:

(1) the effect of the size of the model domain on the simulation. In the simulation of southeastern Australian storms it is necessary to include the upper-level jet stream into the model domain for intensification of the storm to occur. In addition we have found it is

necessary to have an adequately large domain to simulate the correct movement of the system of interest.

(2) the best manner in which to incorporate high resolution terrain on the finer grids. This terrain must be compatible with the terrain on the coarser grids. In the simulation of southeastern Australian storms it is necessary to include the Great Dividing Range through the northern and southern boundaries of the finest meshes. If the fine mesh terrain is not incorporated correctly it is possible to create numerical noise that results, ultimately, in the simulation being of little value. In addition, the filtering of terrain data sets may remove the effects that some of the higher peaks have on the rainfall, as well as causing some changes in the orientation of terrain features. Such changes affect the low-level convergence field simulated by the model. This low-level convergence frequently results in convection and ultimately rain.

(3) the use and sensitivity of the convective parameterisation scheme used in the model, and

(4) the effect of the model initial analyses on the region of development of the extreme precipitation.

Although these experiments have been unsuccessful to date, a number of important lessons have been learnt about the modelling of extreme rainfall events at high resolution. These lessons have been invaluable to the other simulations described herein. In particular the findings from groups (1), (2) and (3) have been used in simulations of southeastern Australian storms while those from (3) were also useful for the tropical cyclone simulations.

The inadequacy of the initial analyses is a major reason behind our inability to model this storm. The analyses used previously are too course (250 km resolution) to capture many of the features which are important to the development of the meteorological system that resulted in the flash flooding over the Illawarra region. Further simulations are planned using the higher resolution, enhanced re-analysis dataset becoming available from ECMWF.

3.5 Summary of Section 3 Results

In this section we have shown that numerical models can be used for quantitative precipitation forecasting (QPF) of southeastern Australian storms and may provide results at a horizontal resolution of 5-10 km. This requires the use of an appropriate mesoscale model (such as RAMS) coupled with a convective parameterisation scheme that is suitable for use at horizontal resolution of 5-10 km. The importance of this approach has not been dealt with here but should be considered if numerical models are to be used for QPF in the future, regardless of whether this is for operational forecasting or as a tool for PMP estimation. Abbs and Lee (1997) discuss this requirement in greater detail and provide examples for the two case studies described above.

A number of similarities exist between the case studies presented here. Both case studies show that the systems are 60-80% efficient at generating moderate rainfall. The generation of heavy rainfall is 80-100% efficient. Both case studies show only a marginal effect of increases in the moisture availability on the precipitation efficiency. In both cases long-lived moderate rain processes are important contributors to the total precipitation produced by the storm.

Increases in the moisture availability result in the rainfall beginning earlier, lasting longer and being more continuous.

Terrain effects are shown to have an effect both on the amount of rainfall that occurs over the higher terrain as well as affecting the distribution of the rainfall due to the "convergence component" of the storm. This is due to changes in the movement of the storm or changes in the low-level wind field (e.g. blocking) when terrain effects are neglected. The temporal variation of the precipitation for these simulations also illustrates that changes in the moisture field feeds back to the dynamics by affecting both the intensity and movement of the storm.

Conclusions for the depth-area analyses are more difficult to make but a commonality exists when compared to the control curve for each case. The control simulation may be thought of as giving the depth-area curve for the actual storm, while the enhanced-moisture simulation provides the depth-area curves for a storm maximised by the moisture while conserving its dynamic integrity. The enhanced moisture storm is associated with a moisture-adjustment factor and the current PMP methodology would multiply the depth-area curves of the control simulation by this factor. If the depth-area curve for the increased moisture simulation lies above that of the control simulation, then the current PMP techniques under-estimates the precipitation as simulated by the model. This relationship is true for all durations. Where this was the case for the case studies presented in this section, the model produces between 15% and 35% more precipitation than the current PMP technique for areas of 50 to 70 km^2. For areas of 500 km^2, the model produces between 5% and 15% more precipitation then the current PMP technique.

The 2-hour PMP values for the Oberon and Chifley Dam catchments, and the 24-hour PMP values for the catchments of the Chifley and Warragamba Dams and the Hawkesbury-Nepean catchment (Pearce *et al.*, 1992, 1993), have also been compared with the model-derived depth-area curves for the east coast low of August 1986. The 2-hour PMP values have been determined using the GSDM (Bureau of Meteorology, 1985). The 24-hour PMP values have been determined using the method outlined in Section 1.2. For both durations the model has been able simulate a small area storm approaching the PMP values for the Oberon and Chifley Dam catchments. For larger areas, the 24-hour PMP values for the Warragamba Dam and the Hawkesbury-Nepean catchments lie well above the depth-area curves for the east coast low of August 1986. This indicates that, for this particular storm, the model has not been able to be maximised to a level approaching a PMP storm. However, it may be possible to maximise other storms to the PMP values for larger areas.

4. Tropical Cyclones

In this Section we will demonstrate that extreme storms, representative of the GTSM, can be modelled using a mesoscale atmospheric model. The events chosen for this study are Tropical Cyclone (T.C.) Connie and T.C. Aivu.

4.1 Model Initialisation

In the simulations discussed here, the numerical model has been initialised using European Centre for Medium-Range Weather Forecasts (ECMWF) analyses that are available at a resolution of 2.5 degrees latitude and longitude. These analyses have been interpolated horizontally and vertically to the coarsest mesh and they also provide the temporal forcing on the lateral boundaries of the coarsest mesh. The data used to initialise T.C. Connie came from a re-analysis of the operational ECMWF data. This re-analysis utilised previously unavailable data collected from the Australian Monsoon Experiment (AMEX) enhanced observing network. In addition to the enhanced observational data base, the re-analysis utilised an upgraded analysis system. The data base was also additionally enhanced relative to the operational system by the use of higher resolution satellite temperature soundings. The enhanced reanalyses were not available for T.C. Aivu.

The terrain used on all meshes was interpolated from a 1/40th degree data set. The sea surface temperatures (SST) were obtained from the ECMWF analyses.

In these simulations the microphysics parameterisation was activated on all grids. In addition, the convective parameterisation scheme developed by Frank and Cohen (1985, 1987) was used on the coarsest mesh.

4.2 Storm 1: T.C. Connie - January 1987

In January 1987 a large international tropical meteorology observing program was based in Darwin. During that time three tropical cyclones occurred, one of which, T.C. Connie, occurred off the Western Australia coast. Connie originated from a low pressure centre that originated over the land and later moved over the sea, intensified, and reached tropical cyclone strength by 1200 UTC on January 17. Connie then moved southwest and continued to intensify, reaching its lowest central pressure (maximum strength) of 950 hPa at 0600 UTC on 19 January. At 0000 UTC on the 18th the central pressure of the cyclone was estimated to be 988 hPa and by 0000 UTC on the 19th had decreased to 962 hPa.

Although T.C. Connie was not a "problem storm" for hydrological purposes, this tropical cyclone was chosen for this study as it was a large, recently occurring system and so provided us with a good subject on which to develop the techniques required to simulate tropical cyclones at high resolution. In addition, T.C. Connie had been simulated by a number of other

researchers (at much lower resolution) and their results gave guidance for evaluation of our earlier experimental, low-resolution simulations.

4.2.1 Validation

(a) High-Resolution Simulation

In these simulations three levels of interactive grid nesting were used. Grid 1 had a horizontal resolution of approximately 50 km, grid 2 approximately 15 km and grid 3 a resolution of 5 km. To conserve computing resources grid 3 was not activated until 8 hours into the simulation.

The mean sea level pressure predicted by the model after 24 hours of simulation is presented in Figure 21. The central pressure of the cyclone at this time is predicted to be 963 hPa compared to the 962 hPa observed. The model predictions locate the centre of the circulation some 50-100 km west of that observed.

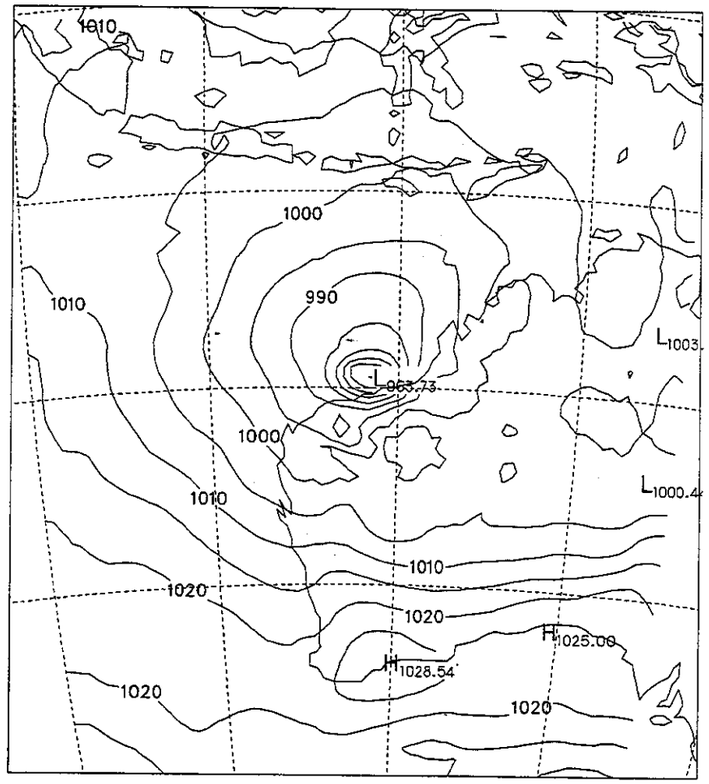

Figure 21: Mean-sea-level pressure (hPa) predicted by the model after 24 hours of simulation.

The paucity of observational data in this region makes validation of the results from the simulation difficult. To alleviate this problem we shall compare the structure of the model predicted rainbands with the conceptual model of a developing rainband based on the work of Ryan *et al.* (1992). From an observational study of the rainband structure in a developing tropical cyclone they found that, horizontally, the rainband was characterised by inflow from both sides of the band with the low-level flow being along the band (Figure 22(a)). The location of the embedded convective cells and their movement over the next few hours is defined by the locus of the vertical velocity maxima. The rainband was observed to be around 80 km wide, but as it matures it narrows to 10-25 km width. They found that in the vertical, the embedded convective cells tilt radially outwards and that the top of the convection occurs at 10 to 12 km height. Observations of the intense convective cells did not reveal organisation into long lived lines.

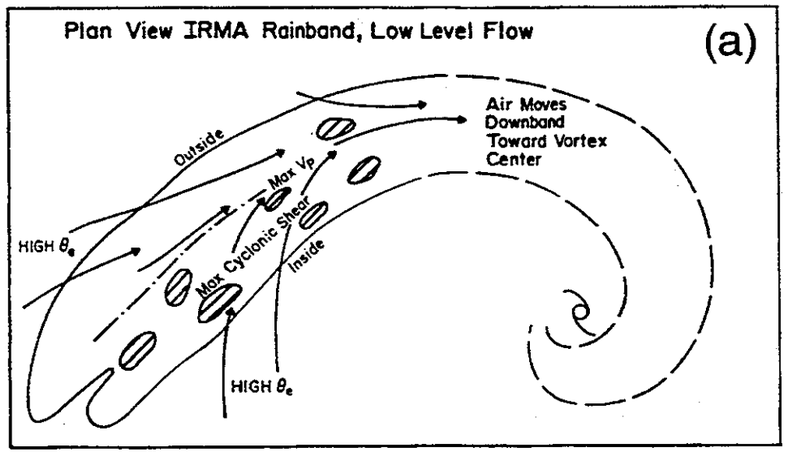

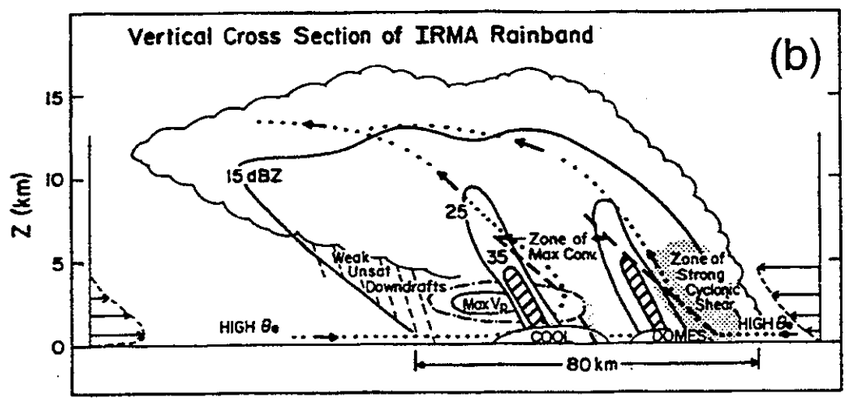

Figure 22: Schematics of (a) a plan view of a developing tropical cyclone rainband and (b) a vertical cross-section through the rainband (from Ryan *et al.*, 1992).

The predicted wind and mixing ratio fields have been used to study the development of rainbands in the modelled tropical cyclone. The location of the model rainband has been defined as the area in which the condensate mixing ratio at a height of 4 km exceeds 0.1 g kg^{-1}. This value corresponds with a radar reflectivity value of approximately 25 dBz, which is the value traditionally used in observational studies to define the location of rainbands. Convective cells have been defined here as those areas in which the 4 km condensate mixing ratio exceeds 1.0 g kg^{-1}. The modelled low-level wind and rainband structure after 12 and 24 hours of simulation are shown in Figure 23. At 12 hours the rainbands are 60 to 80 km wide and contain a number of regions of embedded convection. As in the observations there is inflow from both sides into the band with the low-level flow being along the band into the centre of the cyclone. After 24 hours of simulation pressures have continued to decrease, indicating that the cyclone is intensifying, and a radius of maximum wind has developed that is coincident with a model eye wall. Each of these features is characteristic of an intensifying tropical cyclone. The embedded convection produced in the modelled tropical cyclone also tilts radially outwards from the centre of the system.

The observed and predicted rainfall for the 24 hour period ending 0000 UTC 19 January is shown in Figure 24. The rainfall observations shown here were extracted from Bureau of Meteorology (1991). The features to note are, (i) the large horizontal gradients in both the observed and predicted rainfall on the northern and southern sections of the coastline, (ii) the region of lighter rainfall extending well inland. The main discrepancy between the observed and predicted rainfall appears to be in the location of the eastern band of heavy rainfall. This is possibly because the modelled cyclone had a larger eye (200km compared to 100km) than observed.

The tropical cyclone simulated here appears to resemble observed tropical cyclones in both its structure and evolution, but this simulation was very expensive to perform. Rather than extending the study with an enhanced simulation using this high resolution configuration, we have used the original simulation as a benchmark against which to verify a lower resolution control simulation, and then compare this control simulation with the results from an enhanced moisture simulation.

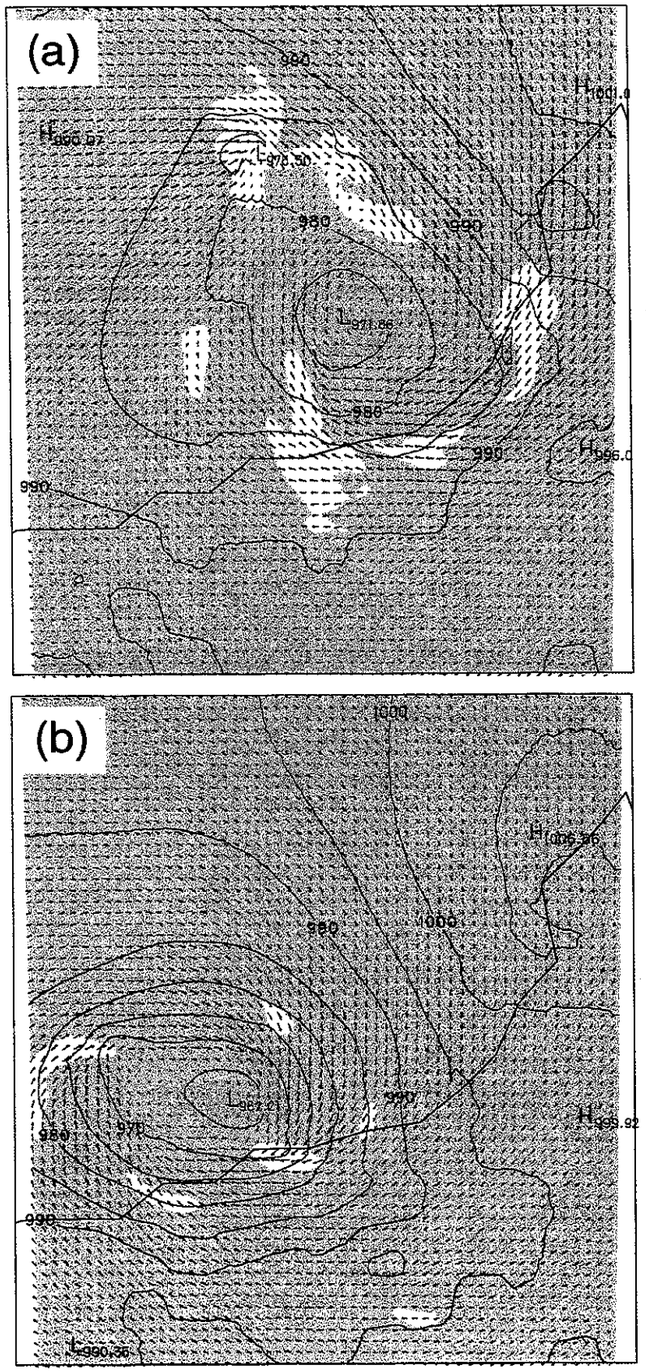

Figure 23: Simulated, horizontal rainband structure after (a) 12 hours of simulation and (b) 24 hours of simulation. Yellow shading denotes areas in which the condensate mixing ratio at a height of 4 km exceeds 0.1 g kg^{-1}, lighter shading where it exceeds 1.0 g kg^{-1}. Also shown are surface wind vectors and mean-sea-level pressure (hPa).

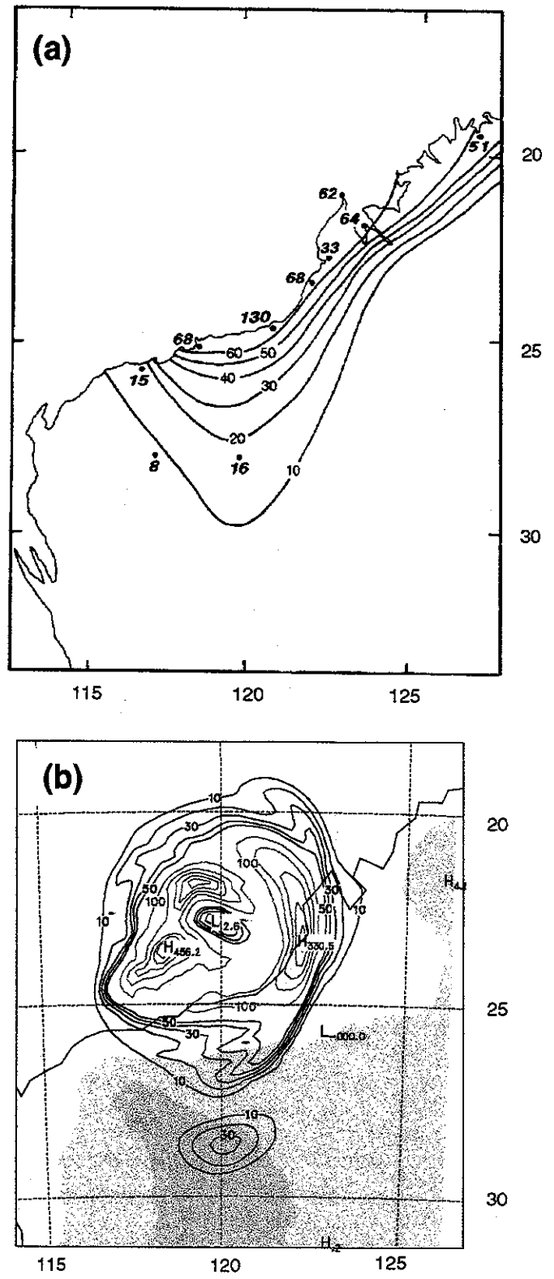

Figure 24: (a) The observed rainfall for the 24 hours ending 00 UTC, 19 January (from Bureau of Meteorology, 1991) and (b) the simulated rainfall for the 24 hours ending 00 UTC, 19 January. The isohyets for the observed rainfall have an interval of 10 mm. For (b) black contours are from 10 to 50 mm with a contour interval of 10 mm. Red contours are for rainfalls greater than 100 mm and have a contour interval of 50 mm. Shading indicates terrain higher than 250 m.

(b) High-Resolution and Control Simulation Comparison

The configuration of the lower resolution control simulation is the same as the high resolution simulation described above, except that in this case we are using only two grids so that the highest resolution achieved by the model in this case is 15 km. A comparison of results from the two simulations shows that the position of the rainband is similar but that the low resolution rainband does not contain regions of embedded convection. After 24 hours the low resolution simulation has not developed an eye-wall-like structure and there is no obvious radius of maximum wind. The secondary rainband structure is similar in both simulations. The low resolution tropical cyclone does not move as rapidly as the high resolution cyclone; this is possibly related to a difference in the wind field between the two simulations such as the lack of a radius of maximum wind.

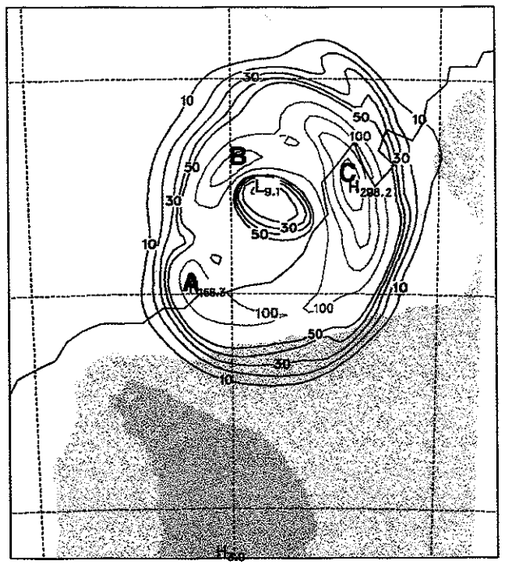

Figure 25: Simulated rainfall for the control simulation for the 24 hours ending 00 UTC, 19 January. Contours are drawn as for Figure 24(b). Shading indicates terrain higher than 250 m.

After 24 hours of simulation the low resolution tropical cyclone has begun to weaken due to the lack of convection at this later time. The precipitation fields produced by the two simulations were qualitatively similar, however, the extreme precipitation produced in the high resolution simulation was approximately 15% greater than that of the low resolution simulation (Figure 25). One of the main conclusions that can be drawn from this comparison is that the majority of the rainfall is due to the stratiform region of the tropical cyclone rainband rather than from the more isolated pockets of embedded convection.

4.2.2 Increased Moisture Simulations

The simulations discussed in this Section have been performed by initialising the model as described above in Section 3.2.2.

Simulations were carried out for dew-point temperature increases of 1.5°C and 3°C. Attempts were also made to perform simulations with dew-point increases of 4 and 5°C, but as before the model produced unrealistic results as the perturbations were too large for the model (see Section 2.1(c)). The successful simulations shall be referred to as CON_+1.5 and CON_+3. The predicted precipitation for these two simulations is shown in Figure 26. The overall distribution of the precipitation is similar for these two simulations and the control simulation, with the maximum precipitation occurring over the land in the eastern half of the tropical cyclone precipitation signature.

Interestingly, as the amount of moisture available to the storm increases, the area over which precipitation occurs decreases. This is particularly obvious for the regions of relatively high precipitation. For the control simulation, a greater area is affected by rainfall higher than 100 mm than for CON_+3.

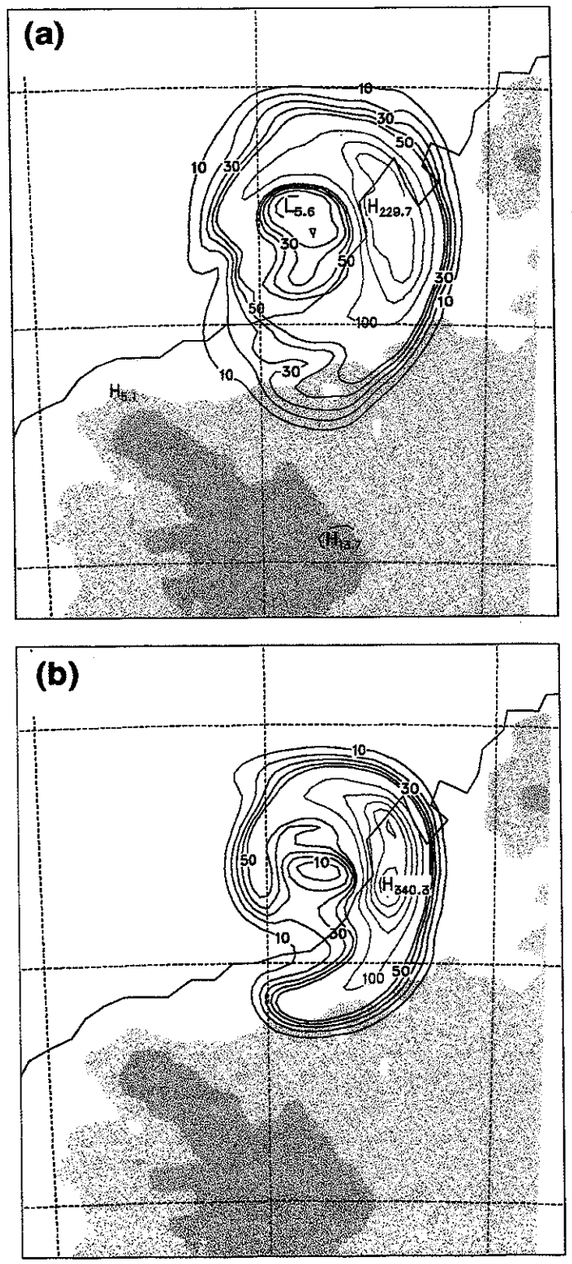

Figure 26: Simulated rainfall for (a) CON_+1.5 and (b) CON_+3. Contours as for Figure 24(b). Shading indicates terrain higher than 250 m.

4.2.3 Storm Efficiencies

Equation (9) has been used to calculate the precipitation efficiencies of the system for (a) the control simulation, (b) CON_+1.5 and (c) CON_+3. As in the previous simulations, the hourly precipitation has been used to partition the storm into heavy and moderate rainfall regions. The temporal variation of PE_c is shown in Figure 27. For each simulation, the system is 60-80% efficient at generating moderate precipitation. For the three simulations, values of PE_c of approximately 100% indicate that the tropical cyclone is very efficient at generating heavy rainfall. For these simulations there is little sensitivity of the precipitation efficiency to increases in the moisture available to the system.

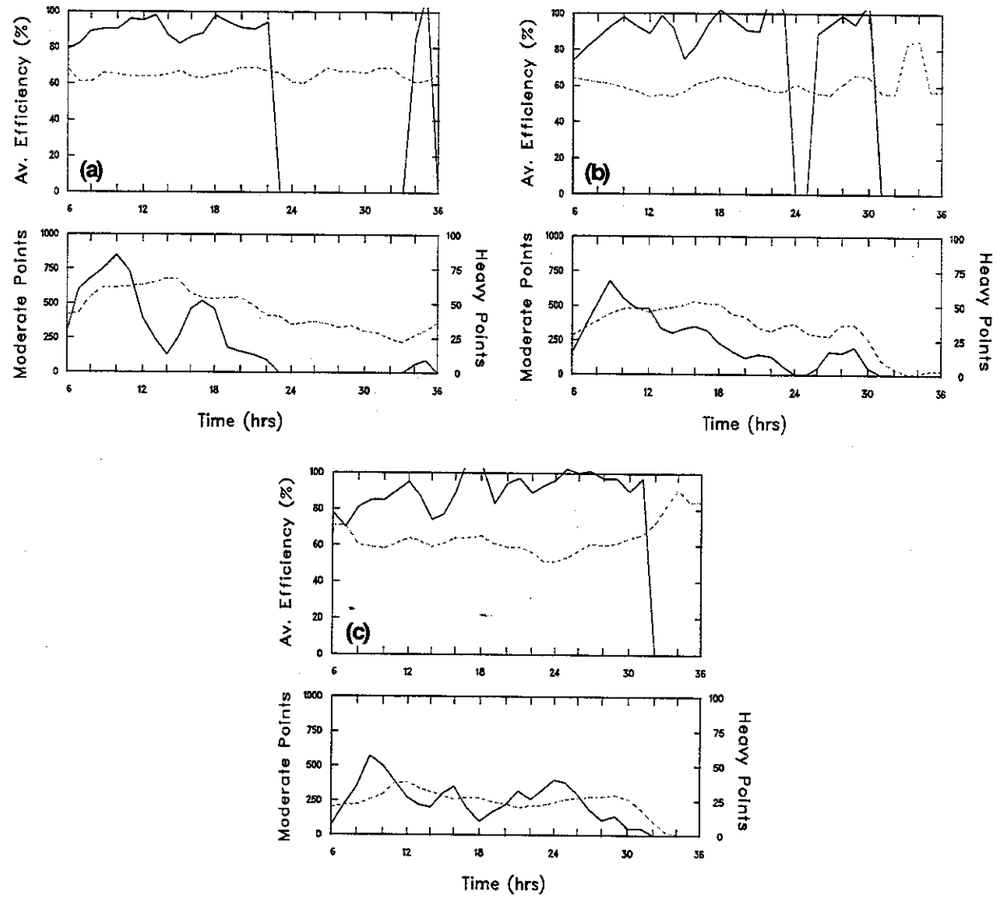

Figure 27: Plots of PE_c for the heavy (solid curve) and moderate (dashed curve) rainfall portions of (a) the control simulation, (b) CON_+1.5 and (c) CON_+3. The lower panels show the number of heavy (solid) and moderate (dashed) rainfall grid points on the finest mesh.

The lower panels of Figure 27 show that, as the moisture available to the storm is increased, heavy rainfall is more continuous and longer lived. However, as the moisture available to the

storm is increased the maximum number of heavy rainfall points decreases. Similarly the number of moderate rainfall grid points decreases as the moisture available to the storm is increased. These results agree with those of Section 4.2.2.

- The percentage of the total rainfall that occurs as heavy rainfall has been calculated for the control simulation, CON_+1.5 and CON_+3 (see Figure 28). As the amount of moisture available to the storm increases, the percentage of heavy rainfall over the land increases. This corresponds with a decrease in the heavy rainfall over the sea, suggesting that the processes that are producing the precipitation are changing as the moisture availability increases.

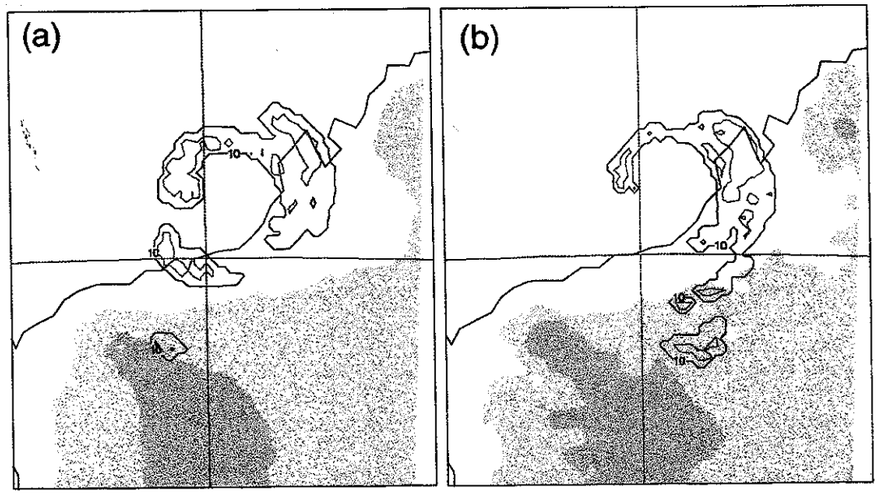

Figure 28: Plots of the percentage of the total rainfall which falls as heavy rainfall (i.e. with an hourly rainfall greater than 25 mm) for (a) the control simulation, (b) CON_+1.5 and (c) CON_+3. Black contours are for 10% and red contours are for 50%.

4.2.4 Temporal Variation of Precipitation

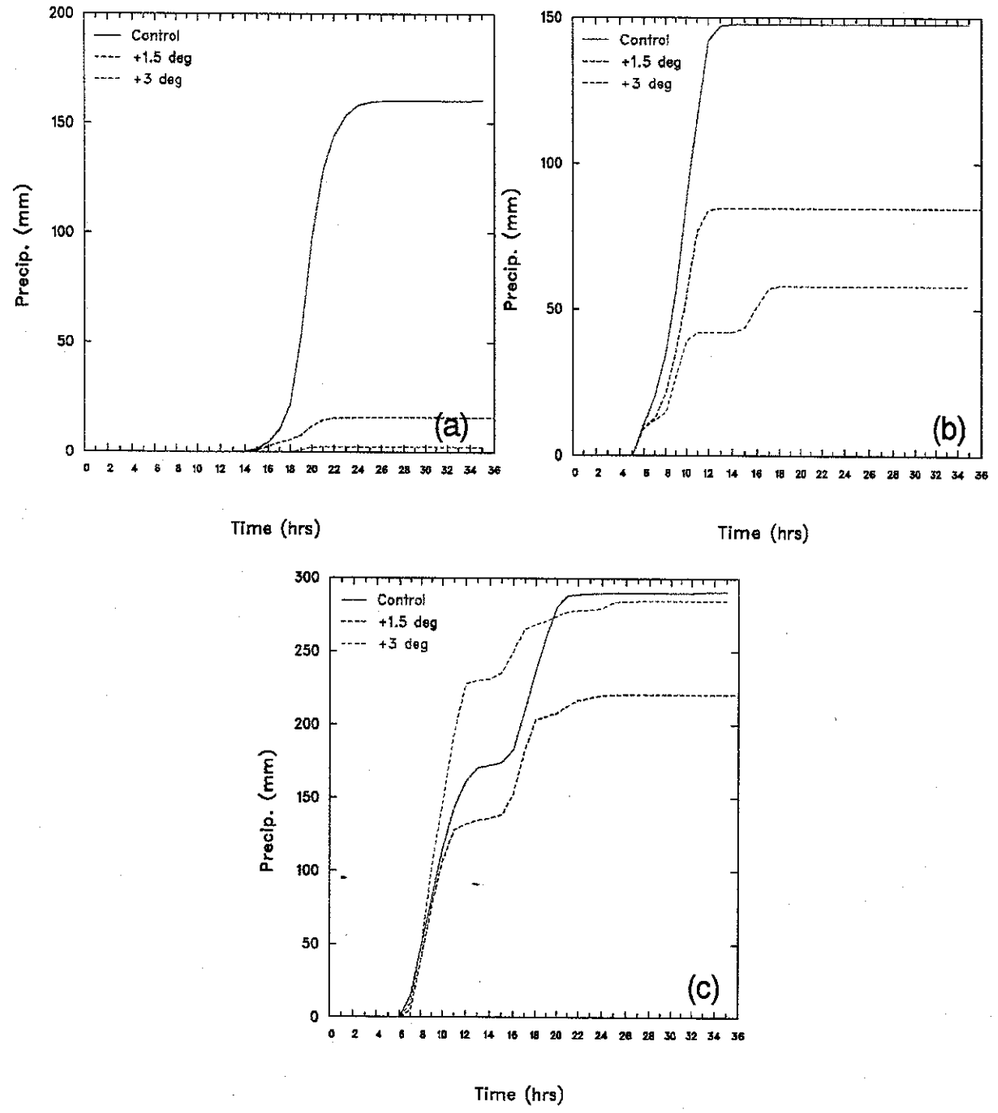

Figure 29: The temporal variation of precipitation at the locations marked (a) "A", (b) "B" and (c) "C" in Figure 25.

The temporal variation of the precipitation has been plotted (Figure 29) for the control simulation, CON_+1.5 and CON_+3. The locations used correspond with the 3 locations marked "A", "B" and "C' in Figure 25.

In general, the temporal variation at each location is similar between simulations. For instance, at site A all precipitation occurs between 14 and 22 hours of the simulation and is the result of a single rainband. At site C the rainfall is due to two rainbands passing across this location. The time of passage of the rainbands is the same for each simulation. Site B exhibits more variation than the other locations. At this location the rainfall for the control simulation and CON_+1.5 is due to an individual rainband but for CON_+3 the accumulated rainfall is due to two, and possibly three, precipitation features.

4.2.5 Depth-Duration-Area Analysis

Depth-area curves have been calculated for standard durations of 2 and 24 hours (Figure 30). For short durations (i.e. 2 hours) the rainfall depths of the control simulation are less than those of both CON_+1.5 and CON_+3 for areas less than about 20000 km^2. For larger areas the reverse is true. For durations of 24 hours the depth-area curve of CON_+1.5 lies below the control curve and that of CON_+3 is above the control curve.

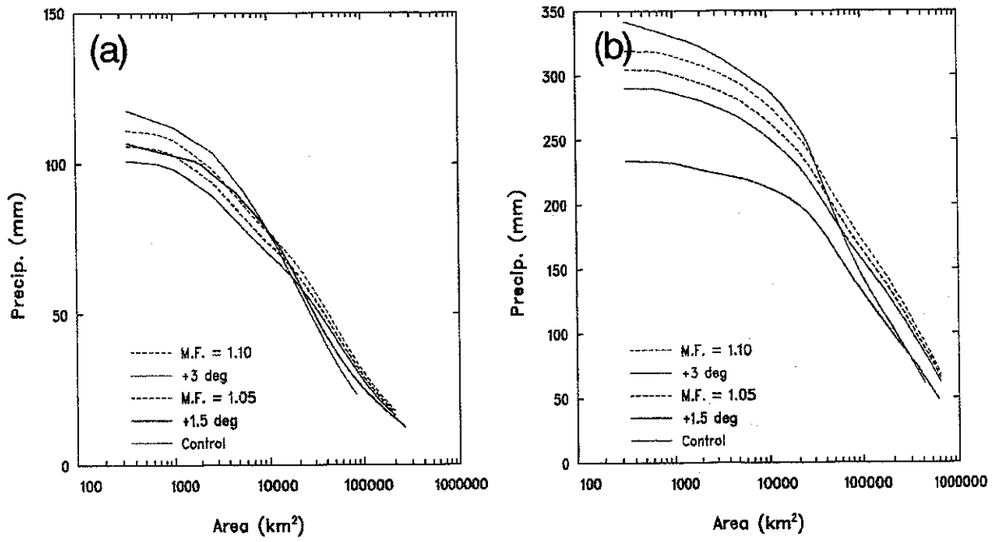

Figure 30: Depth-area curves for (a) 2 hours and (b) 24 hours for the control simulation (solid, red curve), CON_+1.5 (solid, blue curve) and CON_+3 (solid, green curve). Also shown are curves corresponding to maximisation factors of 1.05 (dashed, blue curve) and 1.1 (dashed, green curve).

The maximised curves, corresponding to maximisation factors of 1.05 and 1.1, lie above the depth-area curves of CON_+1.5 and CON_+3 for durations of 2 and 24 hours for areas greater than 20000 km^2. For smaller areas and a duration of two hours, the maximised curves for both cases lie below the corresponding depth-area curves of CON_+1.5 and CON_+3. This is also true for small areas and for a duration of 24 hours for the maximisation factor of 1.1.

For durations of 2 and 24 hours and areas less than approximately 20000 km^2 the current maximisation technique under-estimates the precipitation as predicted by CON_+3. Where this was the case, the model produces between 5% and 10% more precipitation than the current maximisation technique for areas of 300 km^2. For areas greater than approximately 20000 km^2 the current maximisation technique over-estimates the precipitation as predicted by CON_+3. The current technique over-estimates the precipitation predicted in CON_+1.5 for all areas and a duration of 24 hours.

4.3 Storm 2: T.C. Aivu - April 1989

Tropical cyclone Aivu crossed the north Queensland coast near Home Hill on the morning of 4 April 1989. Aivu developed from a tropical low pressure system that formed off the southeast tip of Papua New Guinea on 31 March 1989. Over the next 4 days Aivu moved in a southwesterly direction and intensified. The lowest central pressure during the lifetime of Aivu was estimated to be 935 hPa, 18 hours before the cyclone crossed the coast. The lowest recorded central pressure was 959 hPa. This was recorded in the eye of the cyclone as it crossed the coast. Radar measurements of the eye radius (Bureau of Meteorology, 1990) range from 11 to 17 km as the system crossed the coastline.

Heavy rainfall and major flooding associated with Aivu occurred over large parts of the central Queensland coast and interior. In general, the areas of heaviest precipitation occurred to the south of Aivu's path. In these areas topographic features enhanced the precipitation. The highest daily rainfall for the period (581 mm) occurred at Dalrymple Heights in the mountain ranges to the west of Mackay. The 72-hour total for this station was 1082 mm; this has an average recurrence interval greater than 100 years. The meteorology and impact of this tropical cyclone is described in greater detail in Bureau of Meteorology (1990).

4.3.1 Validation

In these simulations two levels of interactive grid nesting were used. Grid 1 had a horizontal resolution of 48 km and grid 2 a resolution of 12 km.

Mean-sea-level pressure analyses from ECMWF and the model are compared in Figure 31. Neither ECMWF nor the model have been able to capture the rapid deepening of the tropical cyclone prior to its crossing of the north Queensland coastline. A possible reason for this failure is because we have not used a "bogus" vortex to initialise the tropical cyclone. Further discussion of this problem is presented below. The overall evolution of the synoptic-scale flow is captured well by the model. The tropical cyclone crosses the coast at the time observed (see Figure 32), weakens to form a tropical depression as it moves inland over north-western Queensland. By 0000 UTC, 6 April the tropical depression is located well inland and a ridge of high pressure has developed along the coastline. The model predicts stronger ridging than that present in the ECMWF analyses.

Research at GFDL/NOAA at Princeton University (Ross and Kurihara, 1992; Kurihara *et al.*, 1993; Bender *et al.* 1993) has demonstrated that specification of an initial vortex eliminates many of the problems encountered in the numerical simulation of tropical cyclones. These problems include an incorrect position for the tropical cyclone, poor predicted track, inability of the model to "spin-up" a tropical cyclone, and a poor representation of the radius of maximum winds. There are a number of reasons why a bogussed vortex has not been used in our simulations of tropical cyclones. Firstly, initial efforts at simulating a tropical cyclone (T.C. Connie) produced results in which the track of the tropical cyclone was reproduced well and the storm intensified as observed. Much of this success may be due to the high quality of the data set that was used to initialise the model. Secondly, the specification of an initial

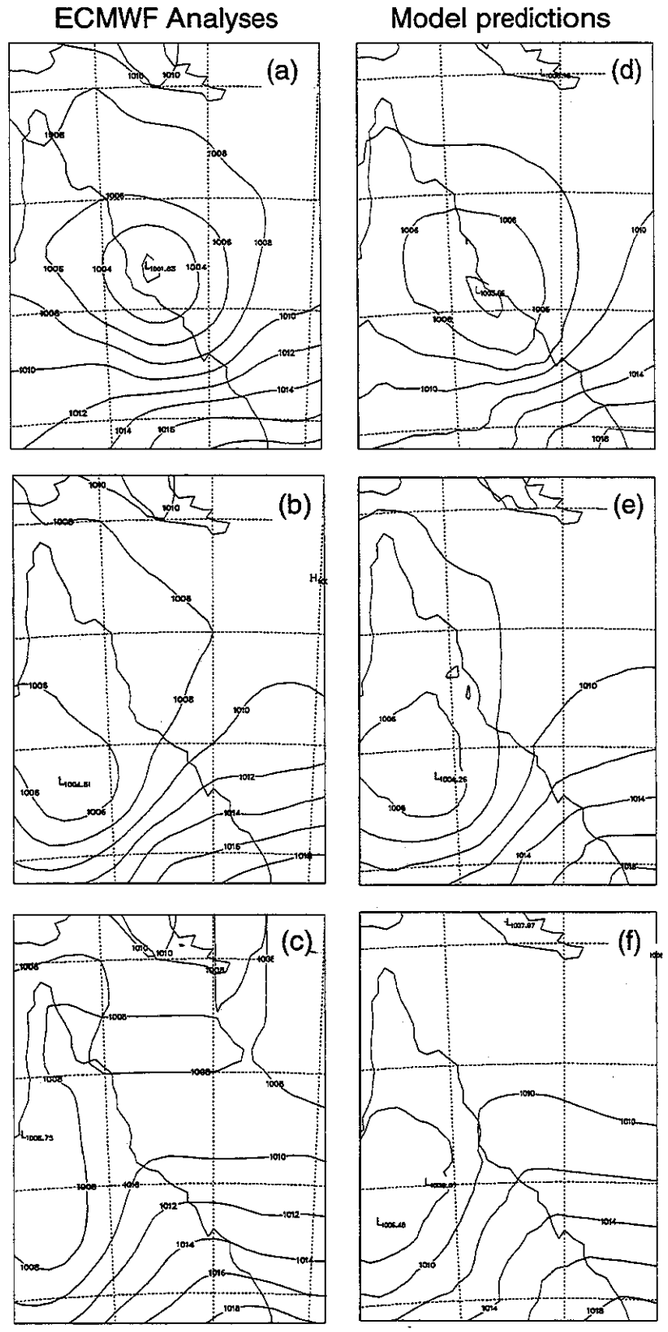

Figure 31: Mean-sea-level pressures (hPa) from the ECMWF analyses for (a) 0000 UTC, 4 April, (b) 0000 UTC, 5 April and (c) 0000 UTC, 6 April and model predicted mean-sea-level pressures for (d) 0000 UTC, 4 April, (e) 0000 UTC, 5 April and (f) 0000 UTC, 6 April.

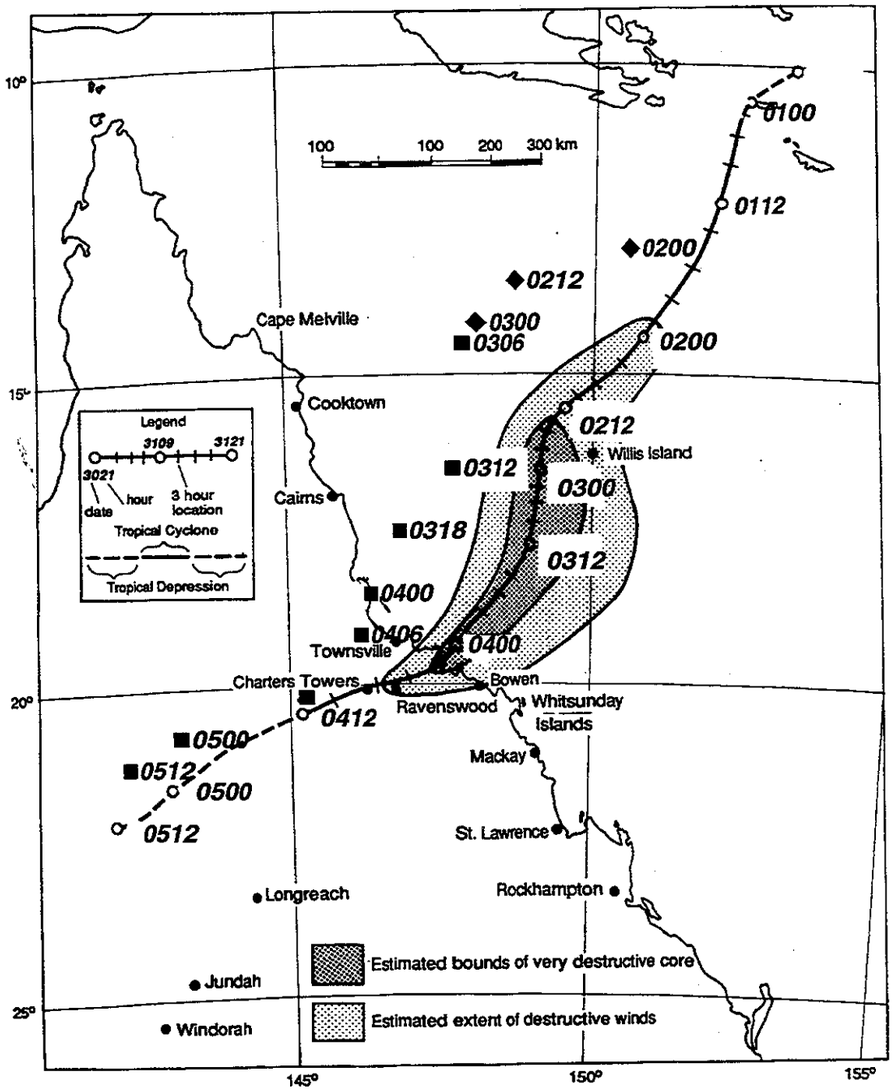

Figure 32: Observed track of T.C. Aivu (from Bureau of Meteorology, 1990). Also included on this figure are the locations of the ECMWF vortex (shown by diamonds) and the predicted track of T.C. Aivu (shown by filled squares).

vortex is not straightforward as a vortex profile needs to be chosen and the maximum wind, radius of maximum wind and central pressure specified. This may produce a realistic simulation of a tropical cyclone if the position of the vortex in the analyses (e.g. ECMWF) is in the correct location. Figure 32 shows that for this case study this was not the case and that the position of the ECMWF vortex between 0000 UTC on 2 April and 0000 UTC 3 April is represented poorly in the analyses. Such problems suggest that a sophisticated approach, similar to that of Ross and Kurihara (1992), would be required to remove the "erroneous"

vortex from the analysis before bogussing in a specified vortex in the correct location. The implementation of such an approach is beyond the scope of the current project. Finally, most of the rainfall produced by T.C. Aivu was due to the strong low-level convergence along the coast coupled with advection of warm, moist air from the ocean. The low-level convergence was enhanced by the local mountainous terrain.

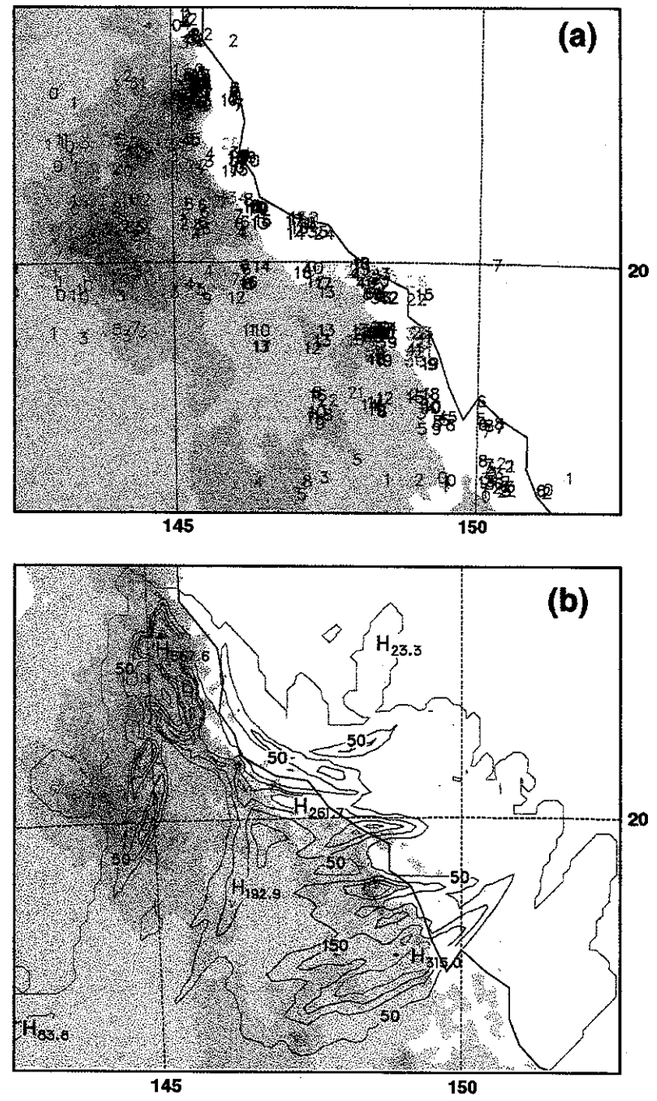

Figure 33: The (a) observed and (b) predicted precipitation for the 72 hours ending 0000 UTC, 6 April. The observed rainfall is colour-coded to correspond with the contours of Figure 33(b). Orange and red colours correspond with precipitation amounts greater than 300 mm. Purple indicates precipitation greater than 600 mm. The contour interval in (b) is 50 mm. Shading indicates terrain higher than 100 m.

The 72-hour precipitation for this event is shown in Figure 33. The numerical model has been able to reproduce the spatial distribution of the area affected by rainfall reasonably well. The location and amounts predicted for the region of high precipitation is not predicted well. The poor representation of the location of the high precipitation region is not surprising considering the poor representation of the track that was in the ECMWF analyses. In both the observations and the simulation, the highest precipitation is located in the high terrain south of the tropical cyclone coastal crossing location. The relatively low predicted rainfall amounts are due to two reasons. Firstly, at a resolution of 12 km, the model is unable to resolve the high topography over which the heavy rain occurred. At this grid resolution the model is resolving features with maximum elevations of approximately 500 m yet the local terrain for this area exceeds 1000 m. Consequently, the model is not producing as much orographically forced ascent as occurred during this event. The second reason is related to the first. The continual supply of warm, moist air coupled with a region of orographically enhanced ascent is favourable to the formation of an orographic cloud that is essentially "anchored" to the orography. The model is not able to resolve this feature at this resolution.

The maximum rainfall amount predicted by the model is 550 mm and occurs much further north than observed. The observed maximum rainfall for this period is 1080 mm. This individual station value has "near-neighbour" values between 600 and 800 mm.

4.3.2 Increased Moisture Simulations

A single increased moisture simulation has been performed for this case study. The model was initialised as described in 3.2.2. A temperature increase of 3°C was used. The simulation did not proceed beyond 63 hours of simulation time as instabilities were generated by the model. The simulation will be referred to as AIVU_+3.

The spatial distribution of the precipitation is very similar for the two cases, however, the locations of the maximum precipitation vary between the simulations. AIVU_+3 also produces more precipitation over the sea. In both cases the highest precipitation is located in the high terrain south of the tropical cyclone coastal crossing location.

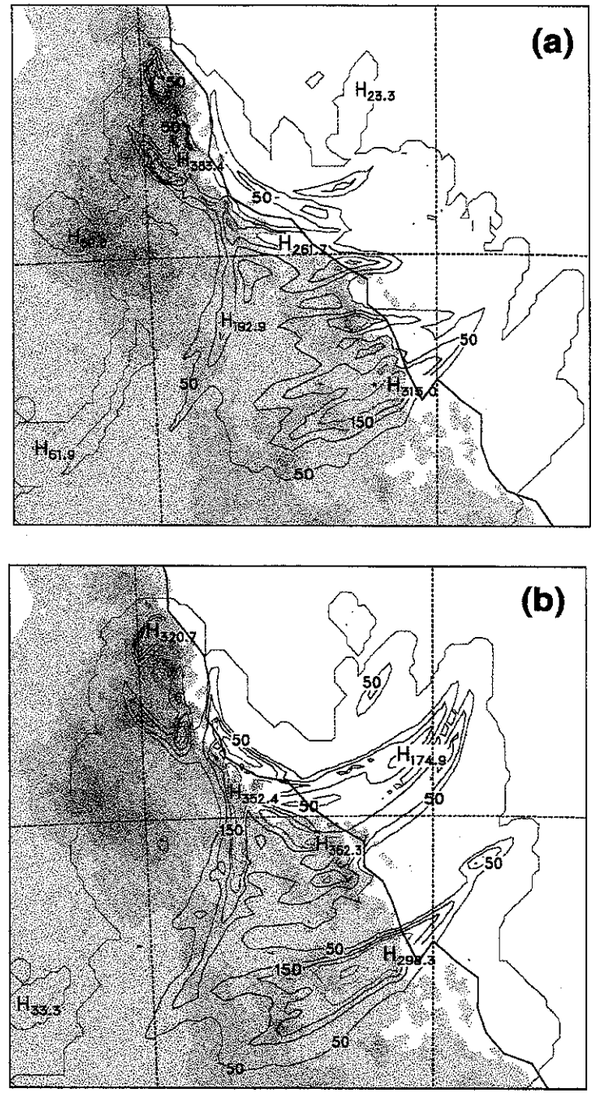

Figure 34: The predicted precipitation for the 60 hours ending 1200 UTC, 5 April for (a) the control simulation and (b) AIVU_+3. Contours and shading as for Figure 33(b).

4.3.3 Storm Efficiencies

Equation (9) has been used to calculate the precipitation efficiencies of the system for both, (a) the control simulation and, (b) AIVU_+3. As for the other case studies, the hourly precipitation rate has been used to partition the storm into heavy and moderate rainfall regions. The temporal variation of PE_c is shown in Figure 35. For both cases the system is 50-70%

efficient at generating moderate rainfall from condensate. For both simulations, heavy rainfall generated by the production of condensate is almost 100% efficient.

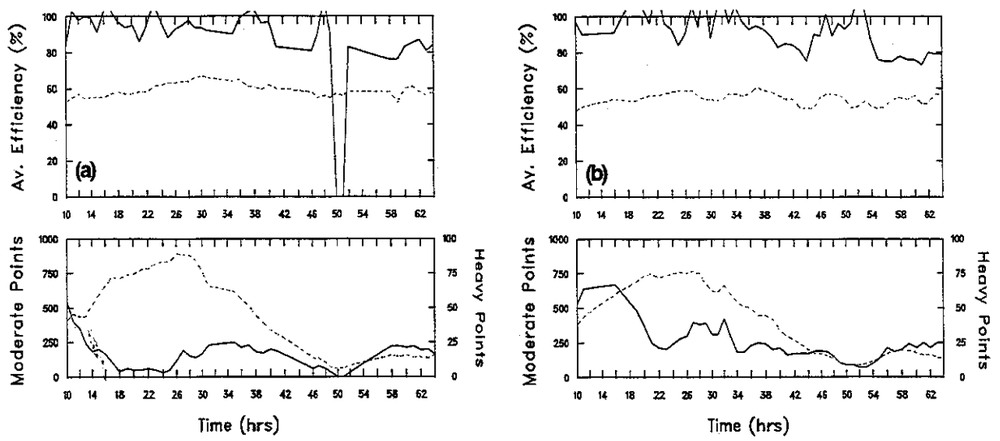

Figure 35: Plots of PE_c for the heavy (solid curve) and moderate (dashed curve) rainfall portions of (a) the control simulation and (b) AIVU_+3. The lower panel shows the number of heavy (solid) and moderate (dashed) rainfall grid points on the finest mesh.

As the moisture available to the system is increased the number of heavy rainfall grid points increases and the heavy rainfall is longer lived.

4.3.4 Depth-Duration-Area Analysis

Depth-area curves have been calculated for standard durations of 2, 24, 36 and 48 hours (Figure 36). These curves are based on the precipitation predicted by the model between 6 and 60 hours of simulation time as AIVU_+3 did not proceed beyond 63 hours of simulation. For all durations, and for areas greater than approximately 1000 km^2, the depth area curve of AIVU_+3 lies above that of the control simulation. For smaller areas the reverse is true. The depth-area curves for AIVU_+3 lie below the corresponding maximised curve, except for a duration of 24 hours. Hence, the current technique tends to over-estimate the predicted precipitation.

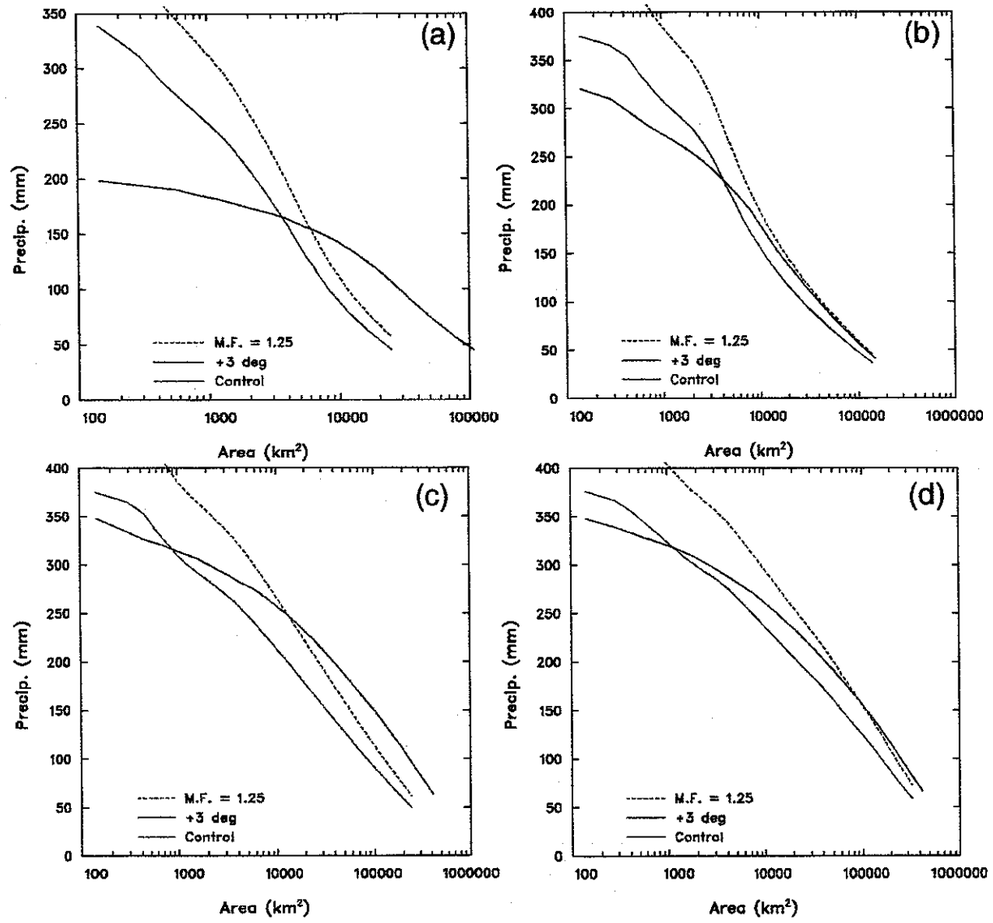

Figure 36: Depth-area analyses for (a) 2 hours, (b) 24 hours, (c) 36 hours and (d) 48 hours for the control simulation (solid, red curve) and AIVU_+3 (solid, blue curve). Also shown is the curve corresponding to a maximisation factor of 1.25 (dashed, blue curve).

4.4 Summary of Section 4 Results

In this section we have shown that the numerical model is able to reproduce many of the high resolution features of tropical cyclones provided that high quality analyses are available with which to initialise the model. We have also found that vortex bogussing techniques should be employed to simulate such features as the formation of a radius of maximum winds, the "spin-up" of the tropical cyclone and a better prediction of the track. Despite these shortcomings, the model is able to provide an adequate prediction of the precipitation field, even at a horizontal resolution of 15 km, against which to test some of the PMP estimation assumptions.

The simulations of tropical cyclone Connie showed that as the moisture available to the storm was increased, the area over which the precipitation occurred decreased. For T.C. Connie and T.C. Aivu, the production of heavy rainfall is almost 100% efficient. There is little sensitivity of the precipitation efficiency to increases in the moisture available to the storm. As the moisture available to the storm is increased, the heavy rainfall becomes more continuous and longer lived.

If the depth-area curve for the increased moisture simulation lies above that of the control simulation, then the current maximisation techniques under-estimates the precipitation as simulated by the model. This relationship is true for all durations, but for T.C. Aivu the relationship only holds for areas greater than approximately 10000 km^2. The reason for the discrepancy in these results for the smaller areas is unknown at this stage but is possibly related to the orography and the resolution used for these simulations. Further simulations are required to investigate the effect of the orography on the distribution of the precipitation produced by T.C. Aivu.

5. Outcomes and Applications

This project has developed techniques so that mesoscale numerical models of the atmosphere may be used as tools for quantitative precipitation forecasting at horizontal scales of 5-10 km. The major application is to use numerical models as a tool to assess some of the assumptions used in the current method of estimating Probable Maximum Precipitation.

These techniques have been tested on four case studies: (i) an east-coast low, (ii) an upper-level cut-off low, (iii) a northwest Australian tropical cyclone, and (iv) a northeast Australian tropical cyclone. For each of these case studies we have investigated the effects increases in the moisture availability have on the precipitation produced by the storm, the precipitation efficiency of the storm and on the depth-duration-area analyses for the storm. We have also investigated the effect of terrain on the distribution of the precipitation produced by the east-coast low and upper-level cut-off low.

5.1 PMP Implications

The increased moisture simulations discussed in this report have been performed by initialising the model from the ECMWF analyses but in these cases the moisture values have been increased by uniformly increasing the temperatures of the atmosphere everywhere, while maintaining the relative humidities. In this way the system under investigation is still in dynamic balance but the specific humidity, and hence the surface dew-point temperature and precipitable water, has been increased. This method is comparable to the technique used to maximise storms in the current PMP approach. A difference between this technique and that currently employed, is that the initial atmosphere in the modelling studies is not necessarily saturated while that used in the current method of estimating PMP is assumed to be saturated through the depth of the atmosphere.

The maximisation factors that result from the technique used in this report lie between 1.1 and 1.3 and are limited by the ability of the numerical model to handle large changes to the initial conditions used by the model. In contrast, Minty *et al.* (1996) calculate values greater than 2 but impose an upper bound of 1.8 on the maximisation factors that are used to estimate the PMP of a storm. The inability of the numerical model to simulate these events with such large maximisation factors raises questions as to the validity of the large maximisation factors for these particular storms. Although the dew-point temperatures associated with these maximisation factors may occur at that particular location and time of year, it needs to be determined if they could actually occur during such extreme precipitation events.

Despite the difference in the upper limit of the maximisation factor that is used for a particular storm, it is still possible to investigate some of the assumptions that are used in the calculation of the PMP. These assumptions are listed in Section 1.3

Five conclusions, with implications for the estimation of PMP, may be drawn from the work presented in our report.

1. As the moisture availability is increased the precipitation efficiency of the storms does not change significantly. For each case study presented in this report, the production of heavy rainfall (rainfall rates greater than 25 mm hr^{-1}) is between 80% and 100% efficient. This supports the simple model that assumes implicitly that extreme precipitation storms have the highest efficiency.
2. As the moisture availability is increased the duration of the heavy rainfall increases, begins earlier and is more continuous. Life cycles are not considered in the simple model, however, the results presented in this report and the recent paper of Zhao *et al.* (1997) suggest that the duration of the storm increases as the moisture availability increases. An increase in the duration of heavy rainfall will result in higher total rainfall.
3. As the moisture availability changes, the spatial distribution of the area over which more than 50% of the total rainfall falls as heavy rainfall changes. Zhao *et al.* (1997) also found that the areal coverage of rainfall varies nonlinearly with the precipitable water.
4. If the depth-area curve for the increased moisture simulation lies above that of the control simulation then the maximisation relationship of the current PMP technique under-estimates the precipitation, compared with that simulated by the model. The simulations reported here indicate that this may occur and hence the precipitation is not linearly related to the precipitable water. For the case studies presented in Section 3, the model produces between 15% and 35% more precipitation than the current storm maximisation technique for areas of 50 to 70 km^2. For areas of 500 km^2, the model produces between 5% and 15% more precipitation then the current storm maximisation technique
5. The topography affects the distribution of the "convergence component" of the precipitation due to feedback effects to the dynamics of the storm system.

Despite these deficiencies in the assumptions used to estimate PMP, we believe that there is no operational replacement available at present for the current PMP methodology. However, improvements in the estimation of PMP may soon be possible if increased effort is placed on (amongst other things) the numerical modelling of extreme rainfall events. These improvements are only possible if the results of these efforts are communicated to, and accepted by, the hydrological community.

5.2 Unanswered questions and problems

The method used in this study to increase the moisture fields was adopted, since it was the method favoured by hydrologists on the project advisory panel and was comparable to the techniques used by the Bureau of Meteorology to maximise storms for PMP estimation. Other methods of maximising the moisture availability should be investigated to determine if the conclusions reached in our study are met. For example, Zhao *et al.* (1996) increase the specific humidity through the depth of the atmosphere to change the precipitable water. Their method, combined with that used here, may allow a wider range of maximisation factors, and higher values, to be tested.

As computing capabilities increase, it will become possible to model extreme storms at increasingly higher resolution. The advances in computing hardware make it possible to examine if further increasing the horizontal resolution of the simulated storms changes the above conclusions.

More case studies should be attempted to determine if the conclusions of Section 5.1 hold true for a wider range of extreme events.

The natural extension of this project is to use the model-predicted precipitation fields to provide an "observed" precipitation field and then subject them to the analysis given to the extreme storms that constitute the GSAM database. After the application of identical maximisation factors, the results of the maximised storm should be compared with that of the equivalent simulated "increased moisture" storm.

More sophisticated initialisation techniques should be developed before more simulations of tropical cyclones are attempted. One such technique that has been used in other studies is known as "vortex bogussing". Following this, the effect of orography on the distribution of precipitation produced in east Australian tropical cyclones should be investigated.

5.3 The future of numerical meteorological models as a tool for hydrological planning

When this project began five years ago it was possible only to perform these simulations on very expensive supercomputers. The continual increase in computing capabilities means that such simulations can now be performed on moderately sized (and priced) workstations.

In addition, a number of re-analysis projects are underway (e.g. NCEP in the USA and at ECMWF) to upgrade the old analyses using state-of-the-art general circulation models and including observations that were not available when the models were originally run. These re-analysis projects are thus providing an improved data set with which to initialise mesoscale numerical models. In the NCEP case the re-analysis extends back to 1970s and so a larger storm database will be available soon.

Finally, the physical parameterisation schemes incorporated into mesoscale numerical models are continually improving, resulting in high quality simulations of these events at increasingly higher horizontal resolution. However, these models are very sophisticated and require a skilled meteorological modeller to manage them and to interpret the results - they cannot be used as a "black box".

Consequently, we believe that it is becoming feasible to perform simulations of a greater number of these events and to provide skilful quantitative precipitation forecasts of them. By utilising a "team approach" in which hydrometeorologists and meteorological modellers work together it is now possible to use mesoscale numerical models as tools for hydrological planning.

6. Appendix

The numerical simulations discussed in this report require large computing resources to be performed. In this appendix we have tabulated the requirements for some of the simulations that have been performed as part of the overall study. Most simulations have been conducted using the Cray Y-MP4E/464 system operated by the CSIRO Supercomputing Support Group. This system has four central processors and 64 Mword of memory. Coupled to the computer is a Storage Technology automated cartridge system (ACS) that provides robotic mounting of cartridge tapes from a silo of tapes.

Listed below is a description of some of the headings used in the table.

CPU time	This is the time required by the computer to perform the simulation.
Real time	This is the actual amount of time required to perform the simulation, from initial submission of the job to completion of the simulation. This time is affected by such factors as (i) the number of other users queued to use the computer, (ii) the memory and time requirements of the job, and (iii) the priority of the job.
Memory	The amount of memory required to perform the simulation.
Data storage	The space required to store the output from the simulation. This is affected by the frequency with which analysis files are saved as well as the size of the simulation itself. For example, if it is anticipated that the results from the simulation will eventually be animated, then analysis files are saved more frequently

The simulation names ECL86, TC2 and TC3 correspond with the control and enhanced moisture simulations of the east coast low of August 1986, the control and enhanced moisture simulations of T.C. Connie and the high resolution (3 grids) simulation of T.C. Connie, respectively.

Simulation name	Simulation time (hrs)	CPU time (hrs)	Real time (months)	Memory (Mwords)	Data storage (Mbytes)
ECL86	36	120	1	17	3000
TC2	24	55	1	14	1450
TC3	24	220	6	25	10100

7. Acknowledgements

This project was initiated by the past Chief of the CSIRO Division of Atmospheric Research, Dr. Brian Tucker, and we thank him for his support and enthusiasm in the "early days" of the project. In addition to the financial support from UWRAA Research Project WR-22 the project has been supported by a number of individuals and organisations. Bill Cotton and Roger Pielke kindly provided the model code for RAMS, developed at Colorado State University under the support of the U.S. National Science Foundation and the Army Research Office. Help and advice from Craig Tremback (Mission Research Corp./*ASTER Division), Bob Walko (CSU) and Jennifer Cram (MESO Corp.), benefited the project investigators in the early use of the model. Alan Dodds and John Andrews of the Sydney Water Corporation were very supportive as the study progressed. Sunhee Lee and Alison Stephens provided computing support for portions of the project. Discussion with Louise Minty from the Hydrology Branch at the Bureau of Meteorology were very helpful in developing our understanding of the current PMP methodology. The Sydney Water Corporation provided the PMP estimates for the Warragamba Dam and Hawkesbury-Nepean Catchments. The NSW Department of Public Works and Services provided the PMP estimates for the catchments of the Oberon and Chifley Dam. The terrain data were supplied by the Australian Surveying and Land Information Group, and Mike Hutchinson from the Centre for Resource and Environmental Studies at ANU. Meteorological data were supplied by the Bureau of Meteorology.

The project has benefited greatly from the suggestions and advice of the project reference panel formed in October 1995:

Russell Mein (Chairman): CRC for Catchment Hydrology, Monash University.
Bruce Stewart: Bureau of Meteorology.
Peter Cloke: Dept. of Public Works and Services, NSW.
John Ruprecht: Water Authority of WA
Brian Taylor: Bureau of Meteorology.

8. References

Abbs, D.J., 1993: Numerical modelling of the Dapto flash flood. BMRC Research Report No. 39, "Modelling severe weather": Papers presented at the fourth BMRC modelling workshop, 26-29 October, 1992. 187-198.

Abbs, D.J. and J.B. Jensen, 1992: Numerical Modeling of Orographically Forced Post-Frontal Rain. *Mon. Wea. Rev.*, **121**, 189-206.

Abbs, D.J. and B.F. Ryan, 1994: UWRAA Research Project WR-22: Numerical Modelling of extreme precipitation events. Mid-project report. 39 pp.

Abbs, D.J. and S.H. Lee, 1997: The use of RAMS as a tool for quantitative precipitation forecasting. Third RAMS Users' Workshop, Echuca, Victoria, Australia. 10-12 July, 1997. 24-27. (available from CSIRO Division of Atmospheric Research).

Australian National Committee on Large Dams (ANCOLD), 1986: Guidelines on Design Floods for Dams, 1986, ANCOLD, Leederville.

Bender, M.A., R.J. Ross, R.E. Tuleya and Y. Kurihara, 1993: Improvements in tropical cyclone track and intensity forecasts using the GFDL initialization system. *Mon. Wea. Rev.*, **121**, 2046-2061.

Bureau of Meteorology, 1984: The estimation of probable maximum precipitation in Australia for short duration and small areas. *Bulletin 51*, AGPS, Canberra, 35 pp.

Bureau of Meteorology, 1987: A report on the heavy rainfall and flood event in the Sydney metropolitan and nearby areas over the period 4-7 August 1986, Special Report, NSW Regional Office, 50 pp.

Bureau of Meteorology, 1990: Report on severe tropical cyclone Aivu: April 1989. Bureau of Meteorology, 44pp.

Bureau of Meteorology, 1991: Climate Data Compact Disc, Space Time Research Pty. Ltd., Melbourne, Australia.

Churchill, D.D., and R.A. Houze, Jr., 1984: Development and structure of winter monsoon cloud clusters on 10 December, 1978. *J. Atmos. Sci.*, **41,** 933-960.

Ferrier, B.S., J. Simpson and W.-K. Tao, 1996: Factors responsible for precipitation efficiencies in midlatitude and tropical squall simulations. *Mon. Wea. Rev.*, **124**, 2100-2125.

Frank, W.L. and C. Cohen, 1985: Properties of tropical cloud ensembles estimated using a cloud model and an observed updraft population. *J. Atmos. Sci.*, **42**, 1911-1928.

Frank, W.L. and C. Cohen, 1987: Simulation of tropical convective systems. Part 1: A cumulus parameterization. *J. Atmos. Sci.*, **44**, 3787-3799.

Golding, B.W. and L.M. Leslie, 1993: The impact of resolution and formulation on model simulations of an east cost low. *Aust. Meteor. Mag.*, **42**, 105-116.

Hart, T.L., 1982: Survey of Probable Maximum Precipitation Using the Synoptic Method of Storm Transposition and Maximisation. Proc. "Workshop on Spillway Design", Melbourne, 1981. AWRC Conf. Ser., **6**, AGPS, Canberra.

Hess, G.D., 1990: Numerical simulation of the August 1986 heavy rainfall event in the Sydney area. *J. Geophys. Res.*, **95**, 2073-2082.

Holland, G.J., A.H. Lynch and L.M. Leslie, 1987: Australian east-coast cyclones. Part I: Synoptic overview and case study. *Mon. Wea. Rev.*, **115**, 3024-3036.

Kurihara, Y., M.A. Bender, R.E. Tuleya and R.J. Ross, 1993: An initialization scheme of hurricane models by vortex specification. *Mon. Wea. Rev.*, **121,** 2030-2045.

Laurenson, E.M. and M.A. Pearse, 1991: Frequency of Extreme Rainfall and Floods. Preprints of papers, "International Hydrology and Water Symposium", **2**, Perth 2-4 October 1991, 392-399.

Leslie, L.M., G.J. Holland and A.H. Lynch, 1987: Australian east-coast cyclones. Part II: Numerical modeling study. *Mon. Wea. Rev.*, **115**, 3037-3053.

Lynch, A.H., 1987: Australian east-coast cyclones. Part III: case study of the storm of August 1986. *Aust. Meteor. Mag.*, **35**, 163-170.

McInnes, K.L. and G.D. Hess, 1992: Modifications to the Australian region limited area model and their impact on an east coast low event. *Aust. Meteor. Mag.*, **40**, 21-31.

McInnes, K.L., L.M. Leslie and J.L. McBride, 1992: Numerical simulation of cut-off lows on the Australian east coast: sensitivity to sea-surface temperature. *Int. J. Clim.*, **12,** 783-795.

Minty, L.J., J. Meighen and M.R. Kennedy, 1996: Development of the Generalised Southeast Australia Method for estimating Probable Maximum Precipitation. Hydrology Report Series No. 4, Bureau of Meteorology. 42pp.

National Research Council, 1994: *Estimating Bounds on Extreme Precipitation Events.* National Academy Press, Washington, D.C.

Pearce, H.J., M.R. Kennedy, N.A. Farnsworth, S.E. Lawrence, J. Meighen, L.H. Turner and B.A. Barlow, 1992: Generalised probable maximum precipitation estimates for the Warragamba Dam catchment., HAS Report No. GSPMP/01, Bureau of Meteorology.

Pearce, H.J., M.R. Kennedy, N.A. Farnsworth, S.E. Lawrence, I.G. Robertson, J. Meighen, L.H. Turner and B.A. Barlow, 1993: Generalised probable maximum precipitation estimates for the Chifley and Oberon Dam catchments., HAS Report No. GSPMP/06, Bureau of Meteorology.

Pearce, H.J. and M.R. Kennedy, 1994: Generalised Probable Maximum Precipitation estimation methods for Australia. *Aust. Civ. Engg. Trans.*, **CE34,** 97-104.

Ross, R.J. and Y. Kurihara, 1992: A simplified scheme to simulate asymmetries due to the beta effect in barotropic vortices. *J. Atmos. Sci.*, **49,** 1620-1628.

Ryan, B.F. and D.J. Abbs, 1991: Quantitative Precipitation Forecasting Using Numerical Models. Land and Water Resources Research and Development Corporation Project S88/40 Final Report, 8pp.

Ryan, B.F., G.M. Barnes and E.J. Zipser, 1992: A wide rainband in a developing tropical cyclone. *Mon. Wea. Rev.*, **120,** 431-447.

Shepherd, D.J. and J.R. Colquhoun, 1985: Meteorological aspects of an extraordinary flash flood event near Dapto, New South Wales. *Aust. Meteor. Mag.*, **33**, 87-102.

Tao, W.K., J. Simpson, C.H. Sui, B. Ferrier, S. Lang, J. Scala, M.-D. Chou and K. Pickering, 1993: Heating, moisture and water budgets of tropical and midlatitude squall lines: comparison and sensitivity to longwave radiation. *J. Atmos. Sci.*, **50**, 673-690.

Tremback, C., G. Tripoli, R. Arritt, W.R. Cotton, and R.A. Pielke, 1986: The Regional Atmospheric Modeling System. Proc. Int. Conf. Development and Applications of Computer Techniques to Environmental Studies, P Zannetti, Ed., November 1986, Los Angeles, U.S.A. Computational Mechanics Publication, Redwood Burn Ltd., Trowbridge, England, 601-607.

Weisman, M.L. and J.B. Klemp, 1982: The dependence of numerically simulated convective storms on vertical wind shear and buoyancy. *Mon. Wea. Rev.*, **110,** 504-520.

Wiesner, C.J. 1970: Hydrometeorology. Chapman and Hall, London, 232pp.

World Meteorological Organisation, 1969: Manual for depth-area-duration analysis of storm precipitation. WMO No. 237, TP 129, Geneva.

Zhao, W., J.A. Smith and A.A. Bradley, 1997: Numerical simulation of a heavy rainfall event during the PRE-STORM experiment. *Water Resour. Res.*, **33**, 783-799.

Zipser, E.J. and M.A. Lemone, 1980: Cumulonimbus vertical velocity events in GATE. Part II: Synthesis and model core structure. *J. Atmos. Sci.*, **37**, 2458-2469.

9. Glossary

AEP	Annual Exceedance Probability
AMEX	Australian Monsoon Experiment
ANCOLD	Australian National Committee On Large Dams
CSU	Colorado State University
DDA Curves	Depth, Duration and Area Curves
ECMWF	European Centre for Medium-Range Weather Forecasts
GSAM	Generalised Southeastern Australian Method
GSDM	Generalised Short Duration Method
GTSM	Generalised Tropical Storm Method
NCEP	National Centers for Environmental Prediction
PMF	Probable Maximum Flood
PMP	Probable Maximum Precipitation
QPF	Quantitative Precipitation Forecasting
RAMS	Regional Atmospheric Modeling System
SST	Sea Surface Temperature
UTC	Universal Time Coordinated

UWRAA RESEARCH REPORTS

Report Number	Title	Author
1	Trickling filter – solids contact process: Pilot plant studies.	M. Laginestra
2	A model of water pricing for Melbourne, Sydney and Perth	P. B. Dixon P. M. Norman
3	Taste generation associated with chloramination	M. Kerslake
4	Bacterial regrowth in water supplies	K. Power L. A. Nagy
5	Leakage management: Assessing the effect of pressure reduction on losses from water distribution systems	B. Horvath
6	Improving communication with the public on water industry policy issues	B. E. Nancarrow G. J. Syme
7	Water use efficiency of domestic appliances	I. J. Beith D. J. Horton
8	Sewage fermentation units to increase degradable COD fraction	P. J. Bliss D. Barnes P. R. Evans I. Law
9	Review of artificial destratification of water storages in Australia	T. F. McAuliffe R. S. Rosich
10	Taste thresholds of mono-chloramine and chlorine in water	R. O'Halloran C. Veres
11	Chromatographic analysis of chloramines using electrochemical detection	R. O'Halloran Hai Lin Ge P. Spizziri
12	Glass reinforced plastic bore casing for large diameter and deep bores	R. Bowyer
13	A guide to improving communication with the public on water industry policy issues	B. E. Nancarrow G. J. Syme
14	Fouling and cleaning of fine bubble ceramic dome diffusers	K. J. Hartley
15	Chloramination of Water Supplies	P. M. Thomas (ed)
16	The 1988 Australian Winter Storms Experiment: Report on aircraft observations	J. B. Jensen
17	Pipeline assets: Life cycle management and economic life	R. Vass M. Anderson R. Lewis D. Samson
18	Development of empirical model for tradewaste discharges to small treatment plants	Camp Scott Furphy
19	PRELIM users guide (Amended): Australian Version	Camp Scott Furphy
20	Chemical regeneration of activated carbon: Preliminary studies	G. Newcombe
21	Management and display of dam surveillance data	D. M. Stirling G. L. Benwell A. B. Murnane
22	Evaluation and demonstration facilities for primary sensors	J. A. Lanaway M. Cavey
23	Modelling and design of reservoir aeration destratification systems	D. P. Lewis J. C. Patterson J. Imberger R. P. Wright S. G. Schadlow
24	Modelling optimum conditions for reservoir destratification using mechanical mixers	R. M. A. Velzeboer J. A. Cugley J. C. Patterson
25	Methods for detection of *Giardia* and *Cryptosporidium* in water: A preliminary assessment	C. A. Bee P. E. Christy B. E. Robinson
26	Toxic cyanobacteria in water supplies: Analytical techniques	D. J. Flett B. C. Nicholson
27	Tracing toxic discharges to sewers by analysis of biofilms	D. Oliver T. Watson
28	Electronic meter reading: Link between water meter and house	P. J. Reid J. S. Renwick M. F. Prior
29	Identification of common noxious cyanobacteria: Part 1 – Nostocales	P. Baker
30	Forecasting water demand using weather data	M. N. Viswanathan
31	Effects of controls on water consumption	M. N. Viswanathan
32	Biological removal of iron from groundwater: Preliminary studies	M. N. Viswanathan
33	Statistical modelling of water main failures	E. Tsui G. Judd
34	Stratification, mixing and water quality in Darwin water supply reservoirs	R. Lukatelich D. Robertson K. Boland J. Imberger J. Patterson
35	Performance auditing in the Australian urban water industry	S. O'Kane I. Parry D. Blunden D. Herring
36	Microbiological studies on enhanced removal of phosphates from sewage	R. C. Bayly J. W. May G. Vasiliadis G. N. Rees
37	Magnetite and microwaves in sewage effluent treatment	D. R. Dixon A. J. Ware
38	Polymer based electrode for the selective detection of dichloramine	Y. Lin G. G. Wallace
39	Current cost asset valuation: Methodology	J. Dyke

UWRAA RESEARCH REPORTS

Report Number	Title	Author
40	Community analysis of household water pressure satisfaction	G. J. Syme B. E. Nancarrow B. J. Bishop P. VanderWal
41	Assessment of coagulants for water treatment	C. Donati
42	Coagulants for water treatment: A generic guide	ACWQR
43	Optimal prices for urban water: A general equilibrium model applied to Melbourne	P.B. Dixon D.J. Baker
44	Applications of the Streaming Current Detector in water treatment	W. Barron D. R. Dixon M. Pascoe
45	Sydney coastal stormwater study	W. G. Rowlands et.al.
46	Identification of common noxious cyanobacteria: Part 2 – Chroococcales and Oscillatoriales	P. Baker
47	Levelling using the Global Positioning System	A. P. Armstrong P. A. Collier F. J. Leahy
48	Allocation of sewerage costs to customer segments	R. Hood P. Geary
49	Impact of urban lawns on nutrient contamination of an unconfined aquifer	M. L. Sharma D. E. Herne P. G. Kin J. D. M. Byrne
50	Early warning system for hazardous substances in sewage	R. O'Halloran B. A. Sexton N. H. Pilkington
51	Management model for trade waste discharges to small treatment plants (including PRELIM VERSION 4.0 Users Guide)	Camp Scott Furphy
52	Automatic meter reading: Link between meters and billing centre (Combined utilities trial)	B. Phey A. Leong Z. Balazic
53	Prediction of perceived odour strength and type from composition of sewage odour mixtures	D. G. Laing A. Eddy D. J. Best
54	Tracer studies using bacteriophage to predict the fate of viruses in the marine community: Preliminary assessments	B. J. Richardson A. L. Charlton S. Currie P. Ashton I. Lowther
55	Development of a water quality analyser suitable for unattended use in rivers and streams	G. W. Skyring I. A. Johns J. A. Cugley
56	Enhancement of nitrification in wastewater lagoons	P. M. Gross
57	Identification of critical water supply assets	PPK Consultants
58	Water in Our Environment: Education Project	H. Breidahl D. Cliffe H. Henderson
59	Electronic household water meter: Investigation into a cost effective design	Z. Balazic A. Leong
60	Domestic greywater reuse: Preliminary evaluation	B. Jeppesen
61	Chemical regeneration of activated carbon: A feasibility study	G. Newcombe
62	Tracing toxic discharges to sewers by analysis of biofilms (Stage 2)	W. H. Lock
63	Production of Jerusalem artichoke hybrids under irrigation using urban wastewater	M. Parameswaran
64	Control of pitting corrosion of copper tubes in potable waters	R. J. Taylor P. H. Cannington
65	Measurement of Total Factor Productivity in major water utilities: Melbourne case study	I. Manning E. Molyneux
66	Assimilable organic carbon as a measure of bacterial growth potential in water supplies	K. C. Tapang M. Drikas L. E. Bennett
67	Simultaneous peak water demands in residential areas	J. Henstridge G. J. Syme B. E. Nancarrow
68	Installation damage: Effect on lifetimes of uPVC pipes subjected to cyclic pressure	L. S. Burn
69	Safety aspects of the design of roadways as floodways	R. J. Keller B. Mitsch
70	Regional development implications of wastewater reuse: Werribee case study	D. Hunter W. Smith L. Nagy P. Jacob
71	Treatment of electroplating wastes using new-generation membrane technology	A. G. Fane Y. R. Shen
72	Stochastic economic approach to headworks augmentation timing	G. Kuczera W. S. Ng
73	Domestic greywater reuse: Overseas practice and its applicability to Australia	B. Jeppesen D. Solley
74	Decision support systems for the water industry: An Object-Oriented approach	J. M. Edwards
75	Chemical characterisation and olfactometric measurement of odours from sewage treatment process units	R. Kaye N. Mulhem D. Stone
76	Utilisation of sewage sludge for minesite rehabilitation: Rix's Creek Mine Trial	C. P. Phillips
77	A benchmarking methodology for the Australian water industry	I.R.C. Eggleton
78	Water quality effects of aeration/ destratification at Harding Reservoir, W.A.	R.S. Rosich T.A. McAuliffe

UWRAA RESEARCH REPORTS

Report Number	Title	Author
79	Heavy metals and organics in domestic wastewater	W. H. Lock
80	Effluent reuse: Land and wet weather storage requirement	J. M. Anderson T.J. Ruge
81	Graphical interactive pipe network analysis program	B.L. Berghout
82	Survey of pipeline rehabilitation techniques	Gutteridge Haskins & Davey
83	Bioavailability of aluminium from drinking water: Co-exposure with foods and beverages	J. Walton G. Hams D. Wilcox
84	Dezincification of brass in potable waters	D. Nicholas
85	Behaviour of aluminium during water treatment	P. Zhang M. McCormick J. Hughes M. Brymner
87	Benchmarking and best practice for urban waterway management	C. Aitken
88	Quantification of factors controlling the development of *Anabaena circinalis* blooms	J.A. Winder D.M.H. Cheng
89	Urban water, markets and the Hilmer reform process	R. Maddock N. Gonzalez
90	Remote sensing electronic device for hydrogen sulphide in the atmosphere	D.G. Laing D. Barnett G.G. Wallace
91	Simultaneous peak flows for medium density residential areas	J. Henstridge G.J. Syme B.E. Nancarrow S. Martens S. Gilbert
92	Die-off of human pathogens in stored wastewater sludge and sludge applied to land	R. Gibbs C. Hu G. Ho I. Unkovich P. Phillips
93	Benchmarking the economic performance of Australian urban water authorities	London Economics
94	Biological Nutrient Removal Plants: Review of Full-Scale Operation	K. Hartley
95	Stormwater Management in Australia: Community Perceptions, Attitudes and Knowledge	B E Nancarrow B S Jorgensen G J Syme
96	Development of a high resolution water quality model	Ch Zoppou S Roberts
97	Landfarming hydrocarbon wastes	W E Razzell P Griffin F Boevink
98	Water treatment plants for small communities	A B Roberts J A DeLaine
99	The role of biofilm and sediment accumulation and of chlorine tolerance in bacterial regrowth	K N Power R P Schneider K C Marshall
100	Phosphorus in Detergents: Its Contribution to Eutrophication in Australian Inland Waters	P Cullen A Heretakis A Herington
101	Disinfection of Wastewater Effluent: A Review of Current Techniques	C Hamilton
102	The effect of irrigation on Blue Gum (*Eucalyptus globulus*) water uptake	R H Froend G W Chester J K Marshall
103	Principles for Setting Developer's Contributions for Urban Water Infrastructure	G A Draper J F Thomas P B Mcleod
104	Epidemiological Evidence of Algal Toxins in Drinking Water and Recreational Waters	O El Saadi D A Steffensen
105	Detection of Cyanobacterial Peptide Toxins by a Non-Radioactive Protein Phosphatase Inhibition Assay	J F Wheldrake A Bilney L Rosenberg
106	Water Treatment Sludge: Potential for Use as a Soil Ameliorant	M Ahmed C Grant J Oades
107	Model Guidelines for Domestic Greywater Reuse for Australia	B Jeppesen
108	Advance Warning of Cyanobacterial Toxicity	A T R Sim J A P Rostas
109	Guidelines on the Quality of Stormwater and Treated Wastewater for Injection into Aquifers for Storage and Reuse	P Dillon P Pavelic
110	The Destruction of Cyanobacterial Peptide Toxins by Oxidants Used in Water Treatment	J Rositano
111	Application of Duckweed in Treating Municipal Wastewater	R A Leng
112	Alternative Overseas Water Treatment and Supply Practices	P Nadebaum N Johnston T Priestley R Vass
113	Ammonia Removal from Siroflo c® STP treated Sewage using Australian Natural Zeolite	N A Booker E L Cooney

UWRAA RESEARCH REPORTS

Report Number	Title	Author
	Environmental Management Guidelines for the Australian Water Industry	S Mills
114	Predicting the Failure Performance of Individual Water Mains	K Mavin
115	Drinking Water Disinfection By-Products Relevant to the 1996 NHMRC/ARMCANZ Guidelines	K L Simpson K P Hayes
116	Sustainable Urban Water Systems: Issues and Opportunities	M Mouritz P Newman
117	Water Sensitive Urban Design: A Tool for Urban Integrated Catchment Management - a Case Study of Bayswater	M Mouritz P Newman
118	An Evaluation of an Integrated Urban Water Management System: Palmyra Case Study	M Mouritz P Newman
119	Critical Evaluation of Domestic Irrigation Equipment	The Australian Irrigation Technology Centre
120	New Concepts in Sludge Dewatering	P Scales S Johnson D Labbett D Dixon
121	Impact on Water Quality of Gross Pollutants	M Abood S J Riley
123	Determination of the Hepatotoxin Cylindrospermopsin Produced by the Cyanobacterium *Cylindrospermopsis Raciborskii*	P M Bond B C Nicholson
124	The Microbiological Oxidation and Removal of Manganese from Drinking Water by a Continuous Recycle Fluidized Bioreactor	L I Sly L Bryant E Larsen D R Dixon
126	Development of a Bioindicator to Measure In-stream Effects of Wastewater Overflows	G Duke A Veenstra-Quah
129	By-Products Formed in the Destruction of Algal Toxins by Oxidants such as Chlorine	J Rositano P M Bond B C Nicholson

Report Number	Title	Author
	Other Reports	
200	Review of Drinking Water Treatment Coagulants	Gutteridge Haskins & Davey
201	Biological Aspects of Aluminium in Food and Water Supply	F Cumming
	Occasional Papers	
No 1	Water Pricing and the Marginal Cost of Water	R Warner
No 2	Systematic Environmental Management in the Water Industry: Toward Best Practice	S Mills
	A Guide to Wetland Invertebrates of Southwestern Australia	J Davis